Antigen specificity shapes antibody functions in tuberculosis.

Joshua R. Miles[1†], Pei Lu[2†], Shuangyi Bai[3], Genesis P. Aguillón-Durán[4], Javier E. Rodríguez-Herrera[5], Bronwyn M. Gunn[3], Blanca I. Restrepo[4,6,7], and Lenette L. Lu[1,2,8]

[1]UT Southwestern Medical Center, Department of Immunology

[2]UT Southwestern Medical Center, Division of Infectious Diseases and Geographic Medicine, Department of Internal Medicine

[3]Paul G. Allen School of Global Health, College of Veterinary Medicine, Washington State University

[4]Department of Epidemiology, School of Public Health, University of Texas Health Science Center at Houston, Brownsville campus, Brownsville, TX, USA

[5]Departamento Estatal de Micobacteriosis, Secretaría de Salud de Tamaulipas, Reynosa 88630, Matamoros 87370, Tamaulipas, México

[6]School of Medicine, South Texas Diabetes and Obesity Institute, University of Texas Rio Grande Valley, Edinburg, TX, USA

[7]I.CARE and Population Health, Texas Biomedical Research Institute, San Antonio, TX, USA

[8]Parkland Health

[†]equal contribution

21 Abstract

22 Tuberculosis (TB) is the number one infectious disease cause of death worldwide due to
23 an incomplete understanding of immunity. Emerging data highlight antibody functions mediated
24 by the Fc domain as immune correlates. However, the mechanisms by which antibody functions
25 impact the causative agent *Mycobacterium tuberculosis (Mtb)* are unclear. Here, we examine
26 how antigen specificity determined by the Fab domain shapes Fc effector functions against *Mtb.*
27 Using the critical structural and secreted virulence proteins *Mtb* cell wall and ESAT-6 & CFP-10,
28 we observe that antigen specificity alters subclass, antibody post-translational glycosylation,
29 and Fc effector functions in TB patients. Moreover, *Mtb* cell wall IgG3 enhances disease
30 through opsonophagocytosis of extracellular *Mtb*. In contrast, polyclonal and a human
31 monoclonal IgG1 we generated targeting ESAT-6 & CFP-10 inhibit intracellular *Mtb*. These data
32 show that antibodies have multiple roles in TB and antigen specificity is a critical determinant of
33 the protective and pathogenic capacity.

34

35 Introduction

36 While antibodies are leveraged for vaccines, diagnostics, and therapeutics in many
37 infectious diseases, their role in tuberculosis (TB) is unclear (*1-9*). Cellular immunity is thought
38 to be the cornerstone of protection (*3, 10*). However, enhanced T cell responses through
39 immune checkpoint inhibitors paradoxically worsen disease (*11, 12*). Moreover, the first large
40 phase IIB clinical trial of the TB vaccine MVA85A designed to boost Th1 and Th17 responses
41 showed no protection (*13*). Subanalyses showed that CD4 T cell responses associated with
42 increased whereas Ag85A IgG linked to decreased risk of disease. Thus, antibodies have the
43 potential to modulate TB and understanding the mechanisms by which antibody functions
44 impact *Mtb* pathogenesis would enable us to leverage this potential more effectively.

45 Antibodies use the Fab domain to recognize antigen and Fc domain to elicit immune cell
46 effector functions (*2, 5*). Fc domain diversity in subclass and post-translational glycosylation
47 regulate binding to activating and inhibitory Fc receptors (FcRs) that initiate downstream
48 signaling and immune cell effector functions (*14-17*). In mice, loss of activating FcR signaling
49 decreases survival after *Mtb* challenge (*18*). Conversely, loss of inhibitory FcR signaling leads to
50 decreased bacterial burden. In humans, the activating FcγRIIIa is associated with protection in
51 latent TB where bacterial burden is undetectable. This contrasts disease in active TB where *Mtb*
52 is identifiable, transmissible, and lethal if untreated (*19*). We have shown that IgG Fc properties
53 and effector functions diverge in latent and active TB (*20, 21*). Moreover, treatment with IgG
54 from latent compared to active TB leads to decreased *Mtb* burden and increased antimicrobial
55 activities in an *in vitro* macrophage model of *Mtb* infection (*20*). These findings suggest that
56 polyclonal antibodies in TB patients differ in the capacities to modulate *Mtb* infection but
57 whether they are protective or disease enhancing remains to be defined.

58 Antigen specificity as determined by the Fab domain impacts Fc effector functions.
59 Changes in the Fab domain alters the ability of the antibody Fc domain to bind to FcRs and
60 initiate effector functions. For influenza and Cryptococcus, this change is sufficient to alter mAb

61 mediated protection (*22-24*). For TB, mAbs that target different *Mtb* surface and cell wall
62 antigens (LAM, PstS1, and heparin-binding hemagglutinin are examples) utilize different FcRs
63 to impact *Mtb* (*25-28*) but what occurs in latent and active TB is not known. To understand how
64 the target of the antibody modulates the ability of the Fc domain to alter *Mtb* pathogenesis, here
65 we use unique *Mtb* antigens to dissect polyclonal antibody Fc effector functions in TB patients.
66

67 Results

68 *Antigen specificity alters the capacity of antibodies to differentiate latent and active TB*

69 We used patient samples from well characterized latent TB infection and active TB
70 disease because these states in the clinical TB spectrum link to protection and disease (Table)
71 (*29*). Groups were matched in age, sex, and Bacillus Calmette-Guérin (BCG) vaccination.
72 Individuals with co-morbid conditions such as HIV and type II diabetes were excluded. Endemic
73 TB negative controls were used to account for exposure to environmental non-tuberculous
74 mycobacteria and other geographical variations that impact immunity (*30-34*).

75 To systematically approach the >4000 *Mtb* protein antigens (*35*), we balanced breadth
76 and specificity with individual and fractions of mixed antigen preparations from bacteria in
77 culture. Since the dominant repertoire of antigens recognized by antibodies in TB is unclear
78 (*36*), many studies use purified protein derivative (PPD) which is mixture of proteins from
79 bacterial culture (*6, 37, 38*). In addition to PPD, we used protein fractions enriched in
80 components of *Mtb* cell wall, cytosol, and secretions into the culture (culture filtrate) (*39-41*) on
81 the premise that localization of the antigen could impact the sensing, processing, and
82 development of antibodies (*26, 27, 42-45*). For specific proteins, we chose the well-studied
83 secreted bacterial virulence factor complexes Ag85A & Ag85B (*46*) and ESAT-6 & CFP-10 (*47*).
84 As a non-*Mtb* control from a common pulmonary pathogen with high seroprevalence in adults,
85 we used respiratory syncytial virus (RSV) (*48*). Together these antigens enabled the evaluation

86 of humoral immunity targeting bacterial structural, metabolic, and immune modulatory functions
87 important for pathogenesis.
88 We first examined the impact of antigen specificity on how IgG titers relate to infection
89 and disease. Only *Mtb* cell wall IgG could distinguish between latent and active TB (Figure 1A),
90 primarily by IgG1 and IgG2 (Figure 1B). In contrast, IgG reactive to PPD, *Mtb* cytosolic proteins,
91 culture filtrate, and Ag85A & Ag85B and ESAT-6 & CFP-10 could not distinguish between
92 clinical TB states (Figure 1A and 1C). ESAT-6 & CFP-10 IgG was even worse than control RSV
93 IgG (Figure 1A, 1C and Supplemental Figure 1). These data are consistent with the poor ability
94 of *Mtb* reactive IgG in serodiagnostics to identify clinical TB (*49, 50*). We focused on *Mtb* cell
95 wall and ESAT-6 & CFP-10 to understand the antibody Fc effector functions linked to IgG
96 reactive to antigens with the most and least capacities to differentiate latent and active TB.
97
98 *Antigen specificity drives differential antibody Fc domain glycosylation in latent and active TB*
99 Antibodies function through diversity of the Fab domain via its antigenic repertoire and
100 the Fc domain from subclass distribution and post-translational N-glycosylation (*2, 14-17*). On a
101 single conserved residue on the IgG Fc domain (N297) is a core biantennary complex of
102 mannose and N-acetylglucosamine (GlcNAc) (Supplemental Figure 2A). Addition and
103 subtraction of galactose, sialic acid, bisecting GlcNAc, and fucose to the core structure
104 generates heterogenous glycoforms. For every individual cohort sample, we measured the
105 glycoforms on IgG reactive to ESAT-6 & CFP-10, *Mtb* cell wall, control RSV, and total bulk IgG
106 Fc domains (Figure 2A, Supplemental Figure 2B) and summarized them (Figure 2B,
107 Supplemental Figure 2C and 2D). We observed that antigen specific differed from total bulk IgG
108 glycans with higher sialic acid, galactose, and bisecting GlcNAc (Figure 2B and Supplemental
109 Figure 2D). Between antigen specific IgG, *Mtb* antigens distinguished themselves from RSV
110 through even higher sialic acid, galactose, and bisecting GlcNAc and lower fucose (Figure 2B
111 and Supplemental Figure 2D). Between *Mtb* antigens, *Mtb* cell wall compared to ESAT-6 &

112 CFP-10 IgG had lower sialic acid and galactose and higher fucose, with the major changes
113 occurring in fucose without sialic acid. These data show that each antigen specificity has a
114 unique glycosylation pattern, consistent with B cell intrinsic rather than extrinsic mechanisms of
115 IgG glycosylation (*51, 52*).
116 We previously reported that IgG glycosylation diverges between latent and active TB
117 (*20, 21, 53-55*). While differences between these two clinical states were observed here (Figure
118 2C), antigen specificity had a greater impact (Figure 2D and Supplemental Figure 2F) in
119 principal components analysis and hierarchical clustering. Thus, antibody glycosylation is
120 influenced by antigen specificity more than clinical TB state.
121
122 *Antibody Fc effector functions diverge more by antigen specificity than latent and active TB*
123 We hypothesized that differences in subclass distribution and Fc N-glycosylation
124 between *Mtb* cell wall and ESAT-6 & CFP-10 IgG indicated divergence in Fc receptor (FcR)
125 binding and immune cell effector functions. We tested this hypothesis by evaluating the ability of
126 antigen specific IgG in each individual TB patient to engage FcRs described to impact TB:
127 FcγRI (*25, 56, 57*), FcγRIIa (*25, 26, 43*), FcγRIIb (*18, 25, 26, 43*), FcγRIIIa (*19, 20, 26*), and
128 FcRn (*27, 58*) (Supplemental Figure 3A). To incorporate adaptor-mediated signaling and
129 feedback, we used the cell-based assays antibody dependent natural killer cell activation
130 (ADNKA) that induces cellular cytotoxicity and antibody dependent cellular phagocytosis
131 (ADCP) (Supplemental Figure 3B and C), both of which are differentially engaged in latent and
132 active TB (*19, 20, 25, 53*). We found that Fc effector functions were defined by antigen
133 specificity more than TB status (Figure 3A and 3B). ADNKA characterized ESAT-6 & CFP-10,
134 ADCP linked to *Mtb* cell wall IgG, and binding to individual FcRs minimally distinguished the
135 antigens by principal components analyses. These data demonstrate that *Mtb* cell wall and
136 ESAT-6 & CFP-10 elicit different IgG engagement of multiple FcRs to induce cell signaling and

137 activation. Moreover, unique subclass and glycosylation resulting in divergent Fc functions show
138 that antigen specificity has the potential to alter the impact of IgG on *Mtb* pathogenesis.
139
140 *Latent and active TB IgG differentially impact Mtb in macrophage infection*
141 To evaluate how antigen specificity alters antibody modulation of *Mtb*, we used *in vitro*
142 macrophage models of infection. This quintessential immune cell niche has the capacity to
143 restrict and also permit bacterial replication (*20, 25, 26, 55, 59-64*). Monoclonal and polyclonal
144 antibodies have been shown to mediate differential uptake of extracellular *Mtb* into the
145 macrophage (*25, 26, 61, 62, 65*). In this cohort, to measure the impact of polyclonal IgG on *Mtb*
146 burden resulting from opsonophagocytosis of extracellular bacteria into the macrophage, we
147 used a virulent *Mtb* H37Rv reporter strain (*Mtb*-276) where luminescence correlates with
148 bacterial burden (Supplemental Figure 4A) (*66, 67*). We used primary human monocyte derived
149 macrophages (pMDM) that express FcRs reported to be involved in TB (FcγRI, FcγRIIa,
150 FcγRIIb, FcγRIIIa, and FcRn). We incubated bacteria with IgG from each individual patient and
151 used the opsonized *Mtb* to infect pMDMs at an MOI=1 (Figure 4A). We used a low MOI to mimic
152 the high infectivity and paucibacillary nature of *Mtb* and limit the macrophage toxic effects of
153 non-physiological high loads of bacteria. We quantified *Mtb* growth after infection and burden
154 (Supplemental Figure 4B) and found lower bacterial burden when opsonized by IgG from
155 individuals with latent compared to active TB (Figure 4B). These data demonstrate that
156 polyclonal IgG from individuals across the spectrum of latent and active TB have properties that
157 alter uptake of extracellular *Mtb* into the macrophage and its subsequent growth.
158 While extracellular bacteria are present during initial stages of infection and in advanced
159 disease with active TB, the majority of *Mtb* is intracellular (*59, 60, 68, 69*). We have previously
160 shown that intracellular *Mtb* is differentially impacted by polyclonal IgG pooled from latent and
161 active TB patients (*20*). Here, we enhanced the resolution by evaluating IgG from each
162 individual latent and active TB patient. We infected macrophages first, washed away the

163 extracellular *Mtb*, then treated the *Mtb* infected macrophages with IgG (Figure 4C). Consistent
164 with prior studies, intracellular *Mtb* burden was lower after treatment with IgG from individual
165 latent compared to active TB patients (Figure 4D). Thus, polyclonal IgG from individuals across
166 latent and active TB have properties that impact intracellular *Mtb* replication after infection has
167 occurred. The data from these extracellular (Figure 4B) and intracellular (Figure 4D) assays
168 were then used to understand how antigen specificity affects IgG modulation of *Mtb*
169 macrophage infection.
170
171 *Mtb cell wall IgG enhances Mtb burden in opsonophagocytosis of extracellular bacteria*
172 To assess the impact of antigen specificity on opsonophagocytosis of extracellular *Mtb*,
173 we evaluated the relationships between antigen specific IgG properties and *Mtb* burden. Using
174 simple linear regression, we found that *Mtb* burden was positively dependent on *Mtb* cell wall
175 IgG3 and binding to high (FcRn and FcγRI) and low (FcγRIIa and FcγRIIb) affinity FcRs (Figure
176 5A). These relationships were not observed with control RSV (Supplemental Figure 5). There
177 were no relationships in the context of intracellular bacteria with antibody treatment after
178 macrophage infection (Figure 5B). To assess the impact of IgG glycosylation on *Mtb* burden, we
179 used multiple linear regression to incorporate the combination of glycosylation and subclass.
180 We found that extracellular and not intracellular *Mtb* burden was enhanced by the absence of
181 sialic acid and presence of fucose on IgG (Figure 5C and 5D, Supplemental Table 1 and 2), the
182 glycans that most significantly distinguished *Mtb* cell wall from ESAT-6 & CFP-10 IgG (Figure
183 2B). As has been reported by others (*25*), these relationships occurred only in latent and not
184 active TB and linked to higher potency of IgG Fc functions (Supplemental Figure 6). These data
185 show that highly potent *Mtb* cell wall IgG enhances bacterial burden by modulating uptake of
186 extracellular *Mtb* into the macrophage.
187
188 *ESAT-6 & CFP-10 IgG inhibits intracellular Mtb*

189 In contrast to *Mtb* cell wall, we observed that ESAT-6 & CFP-10 IgG inhibits *Mtb* (Figure
190 6A and 6B). More specifically, ESAT-6 & CFP-10 IgG1 negatively linked to intracellular bacterial
191 burden and growth (Figure 6C and 6D) while IgG glycosylation was not (Supplemental Figure 6
192 and Supplemental Tables 3 and 4). As with *Mtb* cell wall IgG, the observations for ESAT-6 &
193 CFP10 IgG were made in latent and not active TB but functional potency no different
194 (Supplemental Figure 7). These data suggest that ESAT-6 & CFP-10 IgG in latent TB have the
195 capacity to protect.
196 To test the ability of ESAT-6 & CFP-10 IgG1 to inhibit *Mtb*, we cloned a monoclonal
197 human IgG1 (ESAT-6 mAb) that recognizes ESAT-6, CFP-10, and the combination of antigens
198 (Supplemental Figure 8A-C). Treatment of *Mtb* infected macrophages with the ESAT-6 mAb as
199 compared to isotype control led to decreased intracellular *Mtb* burden in a dose-dependent
200 manner (Figure 6E and 6F and Supplemental Figure 8D and 8E). These data show that IgG
201 recognizing the secreted *Mtb* virulence factors ESAT-6 & CFP-10 function by inhibiting
202 intracellular bacteria after infection has been established.
203
204 Discussion
205 In this study, we use *Mtb* cell wall proteins and the secreted bacterial virulence factors
206 ESAT-6 & CFP-10 to show that antigen specificity alters how antibody Fc effector functions
207 impact *Mtb* pathogenesis. Previous studies using PPD show that different Fc effector functions
208 correlate with protection and disease in latent and active TB. Here, we show that unique
209 antigens within PPD elicit divergent IgG Fc properties in subclass distribution (Figure 1),
210 glycosylation (Figure 2) and Fc effector functions (Figure 3) that change the effect on *Mtb*
211 infection (Figure 4). *Mtb* cell wall IgG enhances disease through opsonophagocytosis of
212 extracellular *Mtb*. This is through IgG3, the subclass with the highest ability to induce Fc
213 receptor binding and effector functions (*70*), and links to FcγRI, FcγRIIa, and FcγRIIb that drive
214 antibody dependent cellular phagocytosis, as well as the high affinity FcRn (Figure 5A). In

215 addition, the presence of sialic acid and absence of fucose on *Mtb* cell wall IgG link to *Mtb*
216 burden (Figure 5C), indicating that glycan modulation of FcR binding as described in the
217 literature is also important (*17, 71-74*). In contrast, ESAT-6 & CFP-10 IgG1 inhibits the
218 intracellular *Mtb* population after infection has occurred (Figure 6B). Its protective capacity is
219 shown in both polyclonal and mAb studies where ESAT-6 & CFP-10 IgG1 alone is sufficient to
220 measurably inhibit bacterial burden (Figure 6E and 6F). These data show that in a single
221 individual TB patient, not all antibodies are equal, and antigen specificity shapes antibody
222 functions that impact *Mtb* pathogenesis.

223 One possible way that different antigens from the same bacteria could elicit divergent
224 antibody Fc properties could be immune priming. *Mtb* cell wall proteins cross-react with
225 environmental NTMs (*30-34, 42*). In comparison, ESAT-6 & CFP-10 are more specific for *Mtb*
226 such that it is used for current T-cell based diagnostics (*75*). As such, *Mtb* cell wall antibody
227 functions could reflect immunity from exposures to both NTM and *Mtb* whereas ESAT-6 & CFP-
228 10 could represent responses only to *Mtb* (*31*). Further studies that assess the effect of pre-
229 existing NTM immunity on avidity to antigen and Fc properties induced by *Mtb* infection would
230 help evaluate this possibility (*30*).

231 Antibodies targeting *Mtb* cell wall antigens have been described in the literature to
232 enhance and inhibit *Mtb*. Monoclonal IgG1 targeting the bacterial surface exposed heparin
233 binding hemagglutinin (HBHA) enhance bacterial entry into epithelial cells and subsequent *Mtb*
234 burden through FcRn (*27*). Monoclonal IgG targeting *Mtb* cell wall proteins (PstS1, HspX, and
235 LpqH) (*26, 76, 77*) and monoclonal and polyclonal IgG targeting the bacterial glycan
236 arabinomannan inhibit *Mtb* through Fc dependent and independent mechanisms (*25, 61, 62,*
237 *65*). Thus, while the overall mixture of *Mtb* cell wall proteins enhances disease in this study, it is
238 likely that within the cell wall fraction, some individual antigens induce protective and others
239 disease enhancing antibodies.

240 Antibody dependent enhancement of infection has been described in viral and bacterial
241 infections (*78-81*) including the intracellular pathogens Legionella (*82*) and Leishmania (*83, 84*)
242 in macrophages that involve cross-reactive and FcR mediated mechanisms. Because *Mtb* is
243 also an intracellular pathogen where macrophages represent an important niche, antibody
244 dependent enhancement of infection has been hypothesized to occur in TB. These data show
245 that *Mtb* cell wall polyclonal IgG engage macrophage FcRs to enhance disease.
246 IgG targeting the secreted virulence factors ESAT-6 & CFP-10 inhibit intracellular
247 bacteria, conferring protection after *Mtb* has established infection (Figure 6B – 6F). Consistent
248 with these findings, the absence and presence of ESAT-6 & CFP-10 in the bacteria is
249 associated with virulence (*85, 86*). Moreover, an anti-ESAT-6 nanobody blocks intracellular *Mtb*
250 replication (*87*). Because the large size of human IgG compared to a nanobody limits cellular
251 penetration, direct neutralization may not be the mechanism of IgG1 mediated bacterial
252 inhibition in an individual TB patient. ESAT-6 & CFP-10 are secreted from *Mtb* and found on the
253 surface of infected host cells (*47, 88, 89*). Thus, it is possible that the secreted nature of these
254 antigens enables immune complex formation, FcR engagement, and induction of effector
255 functions in macrophages to kill intracellular *Mtb*. Our data show that the ability to activate NK
256 cells through FcγRIIIa and induce cellular cytotoxicity highlights ESAT-6 & CFP-10 IgG (Figure
257 3). A similar process could be occurring with macrophages that express FcγRIIIa and carry out
258 cellular cytotoxicity in addition to FcRs facilitating phagocytosis. mAb Fc modifications to
259 enhance and inhibit cellular cytotoxicity could further evaluate these mechanisms of protection
260 (*90*).
261 Notably, only latent and not active TB IgG properties impacted *Mtb* burden (Figure 5 and
262 6). This phenomenon has been reported with arabinomannan specific IgG (*25*) and attributed to
263 higher functional potency. In this study, increased Fc effector functional potency may explain the
264 observations with *Mtb* cell wall, not ESAT-6 & CFP-10 IgG (Supplemental Figure 6). What could
265 explain the phenomenon for ESAT-6 & CFP-10 IgG would be a prozone-like effect from high

266 levels of other *Mtb* reactive IgG in active TB (*91-93*). Additionally, it is possible that differences
267 in antibody functions reflect the continuum of progression and regression in latent TB as
268 compared to the more limited spectrum represented by active TB without antibiotic treatment
269 (*54, 94-96*).

270 What *Mtb* antigens induce antibody functions that impact the clinical outcomes in TB is
271 unclear but essential to understand if we are to harness antibodies for diagnostics, therapeutics,
272 and vaccines. That both pathogenic and protective IgG exist could explain why some passive
273 serum transfer experiments show inhibition while others enhancement of bacterial burden (*6-9*).
274 *Mtb* cell wall and ESAT-6 & CFP-10 reflect a fraction of the *Mtb* antigen repertoire (*35, 36*). This
275 approach could identify the protective and pathogenic potential for additional bacterial antigens
276 in polyclonal antibody responses and enable us to skew humoral immunity towards beneficial
277 rather than harmful effects. This study represents a starting point with IgG from blood.
278 Extending evaluations to IgA and IgM in pulmonary and peripheral responses will highlight
279 isotype and compartment specific distinctions in mucosal (*30, 76, 97-100*) and systemic
280 immunity critical to understanding the many roles of antibodies in TB.
281

282 <u>Materials and Methods</u>

283 *Study design*

284 Adults were recruited from the Texas/Mexico border (2006-2010) (*101*). Latent TB
285 (n=18) was defined by a positive interferon γ release assay (IGRA) TSPOT or QuantiFERON
286 with no history of prior TB diagnosis or treatment, and no clinical signs and symptoms of active
287 TB disease. Active TB (n=19) was defined by sputum acid fast bacilli smear and culture in
288 combination with clinical signs and symptoms of disease. Endemic controls (n=8) were defined
289 by negative TSPOT or QuantiFERON with no history, clinical signs and symptoms, or exposure
290 to TB. To limit confounding variables, groups for latent and active TB were matched by age and
291 sex (*54, 102*), tested negative for HIV and type 2 diabetes as defined by WHO criteria (*103-*

292 *109*), and received <8 days TB treatment (*53, 110*). Written informed consent was obtained
293 from study participants and approved by institutional IRBs.
294
295 *Sample Collection*
296 Blood samples were collected by venipuncture in sodium heparin tubes, plasma isolated
297 by centrifugation, aliquoted, stored at −80°C, and heat-inactivated (30 min, 55C) prior to use.
298
299 *IgG purification*
300 Polyclonal IgG from patient samples was isolated by negative selection via Melon Gel
301 resin (Thermo Fisher), concentrated by ultra-centrifugal filtration (Millipore), and quantified by
302 ELISA (Mabtech) per manufacturers' instructions.
303
304 *Monoclonal hIgG1 plasmid design and construction*
305 An anti-ESAT-6 VH/k sequence (GenBank: LC189555.1 (*111*)) was synthesized and
306 cloned into a pUC19 vector with a human IgG1 Fc domain as previously described in detail (*90*).
307 Donor and destination plasmids were combined in a single digestion-ligation reaction to
308 generate an expression plasmid encoding the heavy and light chains with BsaI-HF (NEB) and
309 T4 ligase (NEB), transformed into Stellar competent cells (Clontech) and selected by
310 kanamycin.
311
312 *Production of monoclonal hIgG1*
313 As previously described (*90*), plasmids were transfected into 293F suspension cells
314 using Polyethylenimine (PEI) (Polysciences). Supernatants were collected 5 days after
315 transfection and IgG was isolated by protein G magnetic beads (16 hours, 4C), eluted using
316 Pierce IgG Elution Buffer (Thermo Fisher), and neutralized with Tris-HCl pH 8.0.
317

318 *Cell lines*

319 NK92 cells expressing human FcγRIIIa (CD16.NK-92) (ATCC) were maintained in α-
320 MEM without nucleosides (Thermo Fisher), 2mM L-glutamine (Thermo Fisher), 1.5g/L sodium
321 bicarbonate (Thermo Fisher), 0.02mM folic acid (Alfa Aesar), 0.2mM inositol (MP Biomedicals),
322 0.1mM β-mercaptoethanol (Thermo Fisher), 100U/mL IL-2 (STEMCELL), 12.5% horse serum
323 (Cytiva), and 12.5% FBS (Gibco), 37C, 5% CO_2. THP-1 cells (ATCC) were cultured in RPMI-
324 1640 (Sigma-Aldrich), 10% FBS, 2mM L-glutamine, and 10mM HEPES (Thermo Fisher), and
325 55μM beta-mercaptoethanol, 37C, 5% CO_2. Freestyle 293F cells (Thermo Fisher) were
326 maintained in a shaking incubator (125RPM, 37C, 8% CO_2) in Freestyle 293F expression
327 medium (Thermo Fisher).

328

329 *Primary human monocyte derived macrophages*

330 Monocytes were isolated from buffy coats obtained from healthy HIV negative adults by
331 CD14 positive selection (Miltenyi) per manufacturer's instructions and matured by adhesion in
332 RPMI-1640, 10% FBS, 2mM L-glutamine, and 10mM HEPES.

333

334 *Mycobacterium tuberculosis H37Rv*

335 A virulent H37Rv (*Mtb*-276) strain expressing luciferase under the P_{hsp60} promotor was
336 cultured using Middlebrook 7H9 (BD) with 0.05% Tween-80 (Millipore) and Zeocin (20μg/mL)
337 (Invivogen) to log-phase at 37C (*66, 67*), washed with PBS, and passed through a 5μm filter
338 (Millipore) to obtain a single cell suspension prior to infection (MOI=1). Enumeration by colony
339 forming units was performed using serial dilutions on 7H10 medium (BD).

340

341 *Antigens*

342 H37Rv purified protein derivative (PPD) (Statens Serum Institute), culture filtrate (BEI),
343 cytosolic proteins (BEI), and cell wall fractions (BEI), as well as ESAT-6 (BEI), CFP-10 (BEI),

344 Ag85A (BEI), Ag85B (BEI) were used as *Mtb* antigens. As controls, respiratory syncytial virus G
345 (BEI) and F (BEI) proteins were used.
346
347 *Quantification of antigen specific IgG and subclasses*
348 Customized Luminex assays were used to measure antigen specific IgG and subclass
349 levels as previously described (*73, 112, 113*). Carboxylated microspheres (Bio-Rad, MC100
350 series) were coupled to protein antigens using an NHS-ester reaction (Thermo Fisher,
351 cat#A32269) following manufacturer's instructions. Serial dilutions of IgG purified from each
352 individual patient sample (0.18, 0.06, 0.02 ug/mL) was added to antigen-coupled beads
353 (18hours, 4C) and washed. PE-conjugated antibodies detecting total IgG (JDC-10, Southern
354 Biotech), IgG1 (4E3, Southern Biotech), IgG2 (HP6002, Southern Biotech), IgG3 (HP60502,
355 Southern Biotech), and IgG4 (HP6025, Southern Biotech), were added (2 hours, room
356 temperature), washed with PBS 0.05% Tween-20, and re-suspended in PBS to acquire
357 fluorescence intensity on Magpix (Luminex). The relative level of antigen specific antibodies was
358 defined as the area under the curve (AUC) calculated from the serial dilutions for each individual
359 sample.
360
361 *Quantification of antigen binding with ESAT-6 mAb*
362 Customized Luminex assays were used to measure antigen binding (*73, 112, 113*).
363 Antigens were coupled to carboxylated microspheres as described above. Serial dilutions of
364 monoclonal hIgG1 (15, 1.5, 0.15 µg/mL) were added to antigen-coupled beads. PE-conjugated
365 anti-human IgG1 was used for detection and fluorescence intensity acquired on Magpix
366 (Luminex) as described above.
367
368 *Isolation of antigen specific and total IgG Fc domains*

369 Antigens were biotinylated using EZ-Link Sulfo-NHS-LC-Biotin (Thermo Fisher) per
370 manufacturer's instructions and coupled to streptavidin beads (NEB). Patient plasma (diluted
371 1:5 in 0.5M NaCl, 20mM Tris-HCl, 1mM EDTA, pH 7.5) was added to antigen-coupled beads for
372 immunoprecipitation of ESAT-6 & CFP-10 (18 hours, 4C), *Mtb* cell wall (2.5 hours, room
373 temperature), and RSV (18 hours, 4C) specific antibodies. For bulk total IgG, protein G beads
374 (Millipore) were used (2 hours, room temperature). IdeZ (NEB) (1.5 hours, 37C) was used to
375 cleave the Fc domain for subsequent glycan isolation.
376
377 *N-linked glycan isolation and quantification*
378 Isolation, labeling, and quantification of N-linked glycosylation are previously described
379 (*73, 113-115*). In brief, isolated Fc domains were denatured (10 minutes, 95C) prior to
380 enzymatic glycan release with PNGaseF (NEB) per manufacturer's instructions (18 hours, 37C).
381 For antigen specific IgG Fc domains, released glycans were isolated with Agencourt CleanSEQ
382 beads (Beckman Coulter). For total bulk IgG Fc domains, proteins were precipitated in ice-cold
383 ethanol. Glycan-containing supernatants were dried using a CentriVap, then labeled with 8-
384 aminoinopyrene-13,6-trisulfonic acid (APTS) (Thermo Fisher) in 1.2M citric acid and 1M
385 $NaBH_3CN$ in tetrahydrofuran (Thermo Fisher), and 0.5% NP-40 (NEB) (3 hours, 55C). Excess
386 APTS was removed using Bio-Gel P-2 size exclusion resin (Bio-Rad) (antigen specific glycans)
387 and Agencourt CleanSEQ beads (total bulk glycans). Labeled samples were run with a LIZ 600
388 DNA ladder (Thermo Fisher) in Hi-Di formamide (Thermo Fisher) on an ABI Gene Analyzer
389 3500XL and analyzed using GlycanAssure version 1.0 (Thermo Fisher).
390
391 *Measurement of antigen specific IgG Fc receptor binding*
392 Customized Luminex assay was used to measure antigen specific IgG FcR binding as
393 previously reported (*73, 112, 113, 116*). As described above, carboxylated microspheres were
394 coupled to protein antigens using an NHS-ester reaction and serial dilutions of IgG purified from

395 each individual patient sample (0.18, 0.06, 0.02 ug/mL) was added to antigen-coupled beads.
396 Recombinant FcRs (FcγRIIIa, FcγRIIa, FcγRIIb, and FcRn) (R&D) were conjugated with
397 phycoerythrin (PE) (Abcam) per manufacturer's instructions. PE-conjugated FcγRIIIa, FcγRIIa,
398 and FcγRIIb were added at pH 7.4; PE-conjugated FcRn at pH 6.0 (*117*) (2 hours, room
399 temperature). FcγRI recombinant protein (R&D) was added to IgG coated beads and then
400 incubated with mouse anti-human FcγRI (10.1, Santa Cruz) (1 hour, room temperature) followed
401 by PE-conjugated goat anti-mouse (Southern Biotech) (1 hour, room temperature) for detection.
402 Fluorescence intensity was acquired on a Magpix instrument (Luminex), and AUC calculated as
403 described above.
404
405 *Antibody dependent cellular phagocytosis*
406 The THP-1 phagocytosis assay of antigen-coated beads is previously described (*73,*
407 *113, 118*). *Mtb* cell wall, ESAT-6 & CFP-10, or RSV antigen mix were biotinylated with EZ-Link
408 Sulfo-NHS-LC-Biotin following manufacturer's instructions and coupled to FluoSpheres
409 NeutrAvidin beads (Molecular Probes) (16 hours, 4C). Antigen-coupled beads were incubated
410 with 100μg/mL polyclonal IgG purified from each patient and then added to THP-1 cells (1x10^5
411 per well) (37°C, 16 hours). After fixation with 4% PFA, bead uptake was measured by flow
412 cytometry on a BD-LSR Fortessa and analyzed by FlowJo v10. Phagocytic scores were
413 calculated as the integrated median fluorescence intensity (MFI) (% bead-positive frequency ×
414 MFI/10,000) (*119*).
415
416 *Antibody dependent natural killer cell activation*
417 Antibody dependent NK cell activation is previously described (*73, 113, 120*). ELISA
418 plates were coated with antigen (300ng/well) (18 hours, 4C), washed 3 times with PBS, blocked
419 with 5% BSA (18 hours, 4C), and then washed 3 times. Purified polyclonal IgG from each
420 patient (100μg/mL) was added (2 hours, 37C), followed by CD16a.NK-92 cells (5×10^4

421 cells/well) with brefeldin A (Biolegend), Golgi Stop (BD Biosciences) and anti-CD107a (H4A3,
422 Biolegend) (5 hours, 37C). Cells were stained with anti-CD56 (5.1H11, Biolegend) and anti-
423 CD16 (3G8, Biolegend) and fixed with 4% PFA. Intracellular cytokine staining to detect IFNγ
424 (B27, Biolegend) and TNFα (Mab11, BD Biosciences) was performed in permeabilization buffer
425 (Biolegend). Markers were measured using a BD LSR Fortessa and analyzed by FlowJo as
426 described above.
427
428 *Macrophage Mtb infections*
429 To test the impact of antibodies on the uptake of extracellular *Mtb* into the macrophage
430 and its subsequent replication, purified IgG from each individual patient was incubated with log-
431 phase *Mtb* (4 hours, 37C). The IgG (100ug/mL) opsonized *Mtb* were used to infect primary
432 human monocyte derived macrophages (5x10^4 cells/well) at an MOI=1.
433 To test the impact of antibodies on intracellular *Mtb* replication, macrophages were first
434 infected with *Mtb* (MOI=1) (14 hours, 37C). Extracellular *Mtb* was then washed off prior to the
435 addition of IgG from each individual patient (100µg/mL).
436 Luminescence was measured using a BioTek Synergy Neo2 Hybrid Multimode Reader
437 plate reader every 24 hours until *Mtb* growth reached stationary phase. Each patient sample
438 was tested in duplicate in three independent experiments using macrophage derived from three
439 different healthy HIV negative donors.
440
441 *Statistics*
442 Data are presented as median with 95% confidence intervals (Figure 1B-C, 4B,4D,
443 Supplemental Figure 1, 3A). Data was analyzed by Mann – Whitney test (Table), Chi-square
444 test (Table), logistic regression (Figure 1A), multiple linear regression to adjust for age and sex
445 (Figure 1B-C, 4B, 4D, Supplemental Figure 1, 3A, 7) and to incorporate multiple antibody
446 features (Figure 5C,5D, Supplemental Tables 1-4, Supplemental Figure 6), Friedman test with

447 adjustment for FDR using a two-stage step-up method of Benjamini, Krieger, and Yekutieli with
448 Q=1% (Figure 2B, and Supplemental Figure 2D), principal components analysis (Figure 2C, 2D,
449 3A-B, Supplemental Figure 2E), hierarchical clustering (Supplemental Figure 2F), simple linear
450 regression (Figure 5A, 5B, 6A, 6B, Supplemental Figure 5A-B), Pearson correlation
451 (Supplemental Figure 4A), and unpaired t-test (Figure 6F) using STATA v16, Graphpad
452 Prism10, and JMP17.2.0. Figures were generated using Graphpad Prism10, R using the ggplot
453 package, Cytoscape v3.9.1, JMP17.2.0, and Biorender.
454
455 Author contributions
456 JM and PL designed and conducted experiments, acquired data, analyzed data, and wrote the
457 manuscript. SB conducted experiments and acquired data. GA and JR provided reagents. BG
458 conducted experiments, acquired data, analyzed data, provided reagents, and wrote the
459 manuscript. BR designed the research study, provided reagents, and wrote the manuscript. LL
460 designed the research study, conducted experiments, acquired data, analyzed data, and wrote
461 the manuscript.
462
463 Conflicts of interest
464 The authors have declared that no conflicts of interests exist.
465
466 Acknowledgements
467 We thank Gabrielle Lessen for her assistance with the in vitro *Mtb* macrophage infection
468 experiments and manuscript editing. We thank Michael Shiloh for helpful comments. We thank
469 study participants and clinical staff from the Secretaria de Salud de Tamaulipas and the Hidalgo
470 Department of State and Health Services for field logistics support. This work is supported by
471 UT Southwestern Disease Oriented Scholars Award (LLL), NIH NIAID 5R01AI158858 (LLL),
472 NIH NIAID R21AI144541 (BIR), and NIH NIAID 5T32AI005284-44 (JRM).

473 References

474 1. M. Grobben, R. A. Stuart, M. J. van Gils, The potential of engineered antibodies for HIV-
475 1 therapy and cure. *Curr Opin Virol* **38**, 70-80 (2019).
476 2. L. L. Lu, T. J. Suscovich, S. M. Fortune, G. Alter, Beyond binding: antibody effector
477 functions in infectious diseases. *Nat Rev Immunol* **18**, 46-61 (2018).
478 3. C. Nunes-Alves *et al.*, In search of a new paradigm for protective immunity to TB. *Nat*
479 *Rev Microbiol* **12**, 289-299 (2014).
480 4. S. M. Carpenter, L. L. Lu, Leveraging Antibody, B Cell and Fc Receptor Interactions to
481 Understand Heterogeneous Immune Responses in Tuberculosis. *Front Immunol* **13**,
482 830482 (2022).
483 5. P. S. Grace, B. M. Gunn, L. L. Lu, Engineering the supernatural: monoclonal antibodies
484 for challenging infectious diseases. *Curr Opin Biotechnol* **78**, 102818 (2022).
485 6. A. J. Jacobs, J. Mongkolsapaya, G. R. Screaton, H. McShane, R. J. Wilkinson,
486 Antibodies and tuberculosis. *Tuberculosis (Edinb)* **101**, 102-113 (2016).
487 7. A. Forget, J. C. Benoit, R. Turcotte, N. Gusew-Chartrand, Enhancement activity of anti-
488 mycobacterial sera in experimental Mycobacterium bovis (BCG) infection in mice. *Infect*
489 *Immun* **13**, 1301-1306 (1976).
490 8. THE RESULTS OBTAINED BY DR. VIQUERAT IN HIS TREATMENT OF
491 TUBERCULOSIS. *Lancet* **144**, 756-757 (1894).
492 9. A. Glatman-Freedman, A. Casadevall, Serum therapy for tuberculosis revisited:
493 reappraisal of the role of antibody-mediated immunity against Mycobacterium
494 tuberculosis. *Clin Microbiol Rev* **11**, 514-532 (1998).
495 10. J. A. Philips, J. D. Ernst, Tuberculosis pathogenesis and immunity. *Annu Rev Pathol* **7**,
496 353-384 (2012).
497 11. K. D. Kauffman *et al.*, PD-1 blockade exacerbates Mycobacterium tuberculosis infection
498 in rhesus macaques. *Sci Immunol* **6**, (2021).
499 12. M. Ahmed, L. B. Tezera, P. T. Elkington, A. J. Leslie, The paradox of immune checkpoint
500 inhibition re-activating tuberculosis. *Eur Respir J* **60**, (2022).
501 13. H. A. Fletcher *et al.*, T-cell activation is an immune correlate of risk in BCG vaccinated
502 infants. *Nat Commun* **7**, 11290 (2016).
503 14. F. Nimmerjahn, J. V. Ravetch, Fcgamma receptors as regulators of immune responses.
504 *Nat Rev Immunol* **8**, 34-47 (2008).
505 15. G. Vidarsson, G. Dekkers, T. Rispens, IgG subclasses and allotypes: from structure to
506 effector functions. *Front Immunol* **5**, 520 (2014).
507 16. P. Bruhns *et al.*, Specificity and affinity of human Fcgamma receptors and their
508 polymorphic variants for human IgG subclasses. *Blood* **113**, 3716-3725 (2009).
509 17. T. T. Wang, IgG Fc Glycosylation in Human Immunity. *Curr Top Microbiol Immunol* **423**,
510 63-75 (2019).
511 18. P. J. Maglione, J. Xu, A. Casadevall, J. Chan, Fc gamma receptors regulate immune
512 activation and susceptibility during Mycobacterium tuberculosis infection. *J Immunol* **180**,
513 3329-3338 (2008).
514 19. R. Roy Chowdhury *et al.*, A multi-cohort study of the immune factors associated with M.
515 tuberculosis infection outcomes. *Nature* **560**, 644-648 (2018).
516 20. L. L. Lu *et al.*, A Functional Role for Antibodies in Tuberculosis. *Cell* **167**, 433-443 e414
517 (2016).
518 21. L. L. Lu *et al.*, Antibody Fc Glycosylation Discriminates Between Latent and Active
519 Tuberculosis. *J Infect Dis* **222**, 2093-2102 (2020).
520 22. J. Mukherjee, G. Nussbaum, M. D. Scharff, A. Casadevall, Protective and nonprotective
521 monoclonal antibodies to Cryptococcus neoformans originating from one B cell. *J Exp*
522 *Med* **181**, 405-409 (1995).

523 23. D. J. DiLillo, G. S. Tan, P. Palese, J. V. Ravetch, Broadly neutralizing hemagglutinin
524 stalk-specific antibodies require FcgammaR interactions for protection against influenza
525 virus in vivo. *Nat Med* **20**, 143-151 (2014).
526 24. M. Brinkhaus *et al.*, The Fab region of IgG impairs the internalization pathway of FcRn
527 upon Fc engagement. *Nat Commun* **13**, 6073 (2022).
528 25. T. Chen *et al.*, Capsular glycan recognition provides antibody-mediated immunity against
529 tuberculosis. *J Clin Invest* **130**, 1808-1822 (2020).
530 26. A. Watson *et al.*, Human antibodies targeting a Mycobacterium transporter protein
531 mediate protection against tuberculosis. *Nat Commun* **12**, 602 (2021).
532 27. N. Zimmermann *et al.*, Human isotype-dependent inhibitory antibody responses against
533 Mycobacterium tuberculosis. *EMBO Mol Med* **8**, 1325-1339 (2016).
534 28. E. Ishida *et al.*, Monoclonal antibodies from humans with Mycobacterium tuberculosis
535 exposure or latent infection recognize distinct arabinomannan epitopes. *Commun Biol* **4**,
536 1181 (2021).
537 29. J. R. Andrews *et al.*, Risk of progression to active tuberculosis following reinfection with
538 Mycobacterium tuberculosis. *Clin Infect Dis* **54**, 784-791 (2012).
539 30. T. S. Dutt *et al.*, Mucosal exposure to non-tuberculous mycobacteria elicits B cell-
540 mediated immunity against pulmonary tuberculosis. *Cell Rep* **41**, 111783 (2022).
541 31. L. Brandt *et al.*, Failure of the Mycobacterium bovis BCG vaccine: some species of
542 environmental mycobacteria block multiplication of BCG and induction of protective
543 immunity to tuberculosis. *Infect Immun* **70**, 672-678 (2002).
544 32. J. A. Shah, C. S. Lindestam Arlehamn, D. J. Horne, A. Sette, T. R. Hawn,
545 Nontuberculous Mycobacteria and Heterologous Immunity to Tuberculosis. *J Infect Dis*
546 **220**, 1091-1098 (2019).
547 33. M. van Dorst *et al.*, Immunological factors linked to geographical variation in vaccine
548 responses. *Nat Rev Immunol* **24**, 250-263 (2024).
549 34. G. F. Black *et al.*, Patterns and implications of naturally acquired immune responses to
550 environmental and tuberculous mycobacterial antigens in northern Malawi. *J Infect Dis*
551 **184**, 322-329 (2001).
552 35. S. T. Cole *et al.*, Deciphering the biology of Mycobacterium tuberculosis from the
553 complete genome sequence. *Nature* **393**, 537-544 (1998).
554 36. C. Hermann, C. G. King, TB or not to be: what specificities and impact do antibodies
555 have during tuberculosis? *Oxf Open Immunol* **2**, iqab015 (2021).
556 37. Y. S. Cho *et al.*, Deciphering the proteome of the in vivo diagnostic reagent "purified
557 protein derivative" from Mycobacterium tuberculosis. *Proteomics* **12**, 979-991 (2012).
558 38. H. Yang, N. A. Kruh-Garcia, K. M. Dobos, Purified protein derivatives of tuberculin--past,
559 present, and future. *FEMS Immunol Med Microbiol* **66**, 273-280 (2012).
560 39. M. Lucas *et al.*, Extraction and Separation of Mycobacterial Proteins. *Methods Mol Biol*
561 **2314**, 77-107 (2021).
562 40. G. R. Hirschfield, M. McNeil, P. J. Brennan, Peptidoglycan-associated polypeptides of
563 Mycobacterium tuberculosis. *J Bacteriol* **172**, 1005-1013 (1990).
564 41. M. G. Sonnenberg, J. T. Belisle, Definition of Mycobacterium tuberculosis culture filtrate
565 proteins by two-dimensional polyacrylamide gel electrophoresis, N-terminal amino acid
566 sequencing, and electrospray mass spectrometry. *Infect Immun* **65**, 4515-4524 (1997).
567 42. C. C. Perley *et al.*, The human antibody response to the surface of Mycobacterium
568 tuberculosis. *PLoS One* **9**, e98938 (2014).
569 43. H. Li *et al.*, Latently and uninfected healthcare workers exposed to TB make protective
570 antibodies against Mycobacterium tuberculosis. *Proc Natl Acad Sci U S A* **114**, 5023-
571 5028 (2017).
572 44. K. Weldingh, P. Andersen, Immunological evaluation of novel Mycobacterium
573 tuberculosis culture filtrate proteins. *FEMS Immunol Med Microbiol* **23**, 159-164 (1999).

45. M. Coppola, T. H. Ottenhoff, Genome wide approaches discover novel Mycobacterium tuberculosis antigens as correlates of infection, disease, immunity and targets for vaccination. *Semin Immunol* **39**, 88-101 (2018).
46. J. T. Belisle *et al.*, Role of the major antigen of Mycobacterium tuberculosis in cell wall biogenesis. *Science* **276**, 1420-1422 (1997).
47. P. S. Renshaw *et al.*, Structure and function of the complex formed by the tuberculosis virulence factors CFP-10 and ESAT-6. *EMBO J* **24**, 2491-2498 (2005).
48. J. S. McLellan, W. C. Ray, M. E. Peeples, Structure and function of respiratory syncytial virus surface glycoproteins. *Curr Top Microbiol Immunol* **372**, 83-104 (2013).
49. O. World Health. (World Health Organization, Geneva, 2011), chap. WHO/HTM/TB/2011.5
19 p.
50. K. R. Steingart *et al.*, Commercial serological tests for the diagnosis of active pulmonary and extrapulmonary tuberculosis: an updated systematic review and meta-analysis. *PLoS Med* **8**, e1001062 (2011).
51. M. B. Jones *et al.*, B-cell-independent sialylation of IgG. *Proc Natl Acad Sci U S A* **113**, 7207-7212 (2016).
52. A. Schaffert *et al.*, Minimal B Cell Extrinsic IgG Glycan Modifications of Pro- and Anti-Inflammatory IgG Preparations in vivo. *Front Immunol* **10**, 3024 (2019).
53. P. S. Grace *et al.*, Antibody Subclass and Glycosylation Shift Following Effective TB Treatment. *Front Immunol* **12**, 679973 (2021).
54. L. R. L. Davies *et al.*, Age and sex influence antibody profiles associated with tuberculosis progression. *Nat Microbiol*, (2024).
55. L. L. Lu *et al.*, IFN-gamma-independent immune markers of Mycobacterium tuberculosis exposure. *Nat Med* **25**, 977-987 (2019).
56. M. Ahmed *et al.*, Immune correlates of tuberculosis disease and risk translate across species. *Sci Transl Med* **12**, (2020).
57. M. P. La Manna *et al.*, Quantitative and qualitative profiles of circulating monocytes may help identifying tuberculosis infection and disease stages. *PLoS One* **12**, e0171358 (2017).
58. A. Vogelzang *et al.*, Neonatal Fc Receptor Regulation of Lung Immunoglobulin and CD103+ Dendritic Cells Confers Transient Susceptibility to Tuberculosis. *Infect Immun* **84**, 2914-2921 (2016).
59. M. S. Glickman, W. R. Jacobs, Jr., Microbial pathogenesis of Mycobacterium tuberculosis: dawn of a discipline. *Cell* **104**, 477-485 (2001).
60. P. Chandra, S. J. Grigsby, J. A. Philips, Immune evasion and provocation by Mycobacterium tuberculosis. *Nat Rev Microbiol* **20**, 750-766 (2022).
61. T. Chen *et al.*, Association of Human Antibodies to Arabinomannan With Enhanced Mycobacterial Opsonophagocytosis and Intracellular Growth Reduction. *J Infect Dis* **214**, 300-310 (2016).
62. Y. Liu *et al.*, Features and protective efficacy of human mAbs targeting Mycobacterium tuberculosis arabinomannan. *JCI Insight* **8**, (2023).
63. L. E. DesJardin *et al.*, Mycobacterium tuberculosis-infected human macrophages exhibit enhanced cellular adhesion with increased expression of LFA-1 and ICAM-1 and reduced expression and/or function of complement receptors, FcgammaRII and the mannose receptor. *Microbiology (Reading)* **148**, 3161-3171 (2002).
64. S. B. Cohen *et al.*, Alveolar Macrophages Provide an Early Mycobacterium tuberculosis Niche and Initiate Dissemination. *Cell Host Microbe* **24**, 439-446 e434 (2018).
65. S. K. Kumar, P. Singh, S. Sinha, Naturally produced opsonizing antibodies restrict the survival of Mycobacterium tuberculosis in human macrophages by augmenting phagosome maturation. *Open Biol* **5**, 150171 (2015).

625 66. N. Andreu *et al.*, Optimisation of bioluminescent reporters for use with mycobacteria.
626 *PLoS One* **5**, e10777 (2010).
627 67. E. B. Irvine *et al.*, Fc-engineered antibodies leverage neutrophils to drive control of
628 Mycobacterium tuberculosis. *bioRxiv*, 2022.2005.2001.490220 (2022).
629 68. D. R. Hoff *et al.*, Location of intra- and extracellular M. tuberculosis populations in lungs
630 of mice and guinea pigs during disease progression and after drug treatment. *PLoS One*
631 **6**, e17550 (2011).
632 69. R. Hernandez-Pando *et al.*, Persistence of DNA from Mycobacterium tuberculosis in
633 superficially normal lung tissue during latent infection. *Lancet* **356**, 2133-2138 (2000).
634 70. T. Damelang, S. J. Rogerson, S. J. Kent, A. W. Chung, Role of IgG3 in Infectious
635 Diseases. *Trends Immunol* **40**, 197-211 (2019).
636 71. R. L. Shields *et al.*, Lack of fucose on human IgG1 N-linked oligosaccharide improves
637 binding to human Fcgamma RIII and antibody-dependent cellular toxicity. *J Biol Chem*
638 **277**, 26733-26740 (2002).
639 72. C. Ferrara *et al.*, Unique carbohydrate-carbohydrate interactions are required for high
640 affinity binding between FcgammaRIII and antibodies lacking core fucose. *Proc Natl*
641 *Acad Sci U S A* **108**, 12669-12674 (2011).
642 73. T. A. Bates *et al.*, BNT162b2-induced neutralizing and non-neutralizing antibody
643 functions against SARS-CoV-2 diminish with age. *Cell Rep* **41**, 111544 (2022).
644 74. R. Vattepu, S. L. Sneed, R. M. Anthony, Sialylation as an Important Regulator of
645 Antibody Function. *Front Immunol* **13**, 818736 (2022).
646 75. M. Pai *et al.*, Gamma interferon release assays for detection of Mycobacterium
647 tuberculosis infection. *Clin Microbiol Rev* **27**, 3-20 (2014).
648 76. A. C. Tran *et al.*, Mucosal Therapy of Multi-Drug Resistant Tuberculosis With IgA and
649 Interferon-gamma. *Front Immunol* **11**, 582833 (2020).
650 77. S. Krishnananthasivam *et al.*, An anti-LpqH human monoclonal antibody from an
651 asymptomatic individual mediates protection against Mycobacterium tuberculosis. *NPJ*
652 *Vaccines* **8**, 127 (2023).
653 78. S. Bournazos, A. Gupta, J. V. Ravetch, The role of IgG Fc receptors in antibody-
654 dependent enhancement. *Nat Rev Immunol* **20**, 633-643 (2020).
655 79. S. B. Halstead, S. Mahalingam, M. A. Marovich, S. Ubol, D. M. Mosser, Intrinsic
656 antibody-dependent enhancement of microbial infection in macrophages: disease
657 regulation by immune complexes. *Lancet Infect Dis* **10**, 712-722 (2010).
658 80. V. V. L. Torres, C. F. Coggon, T. J. Wells, Antibody-Dependent Enhancement of
659 Bacterial Disease: Prevalence, Mechanisms, and Treatment. *Infect Immun* **89**, (2021).
660 81. N. A. Kuzmina *et al.*, Antibody-Dependent Enhancement of Ebola Virus Infection by
661 Human Antibodies Isolated from Survivors. *Cell Rep* **24**, 1802-1815 e1805 (2018).
662 82. R. H. Widen, C. A. Newton, T. W. Klein, H. Friedman, Antibody-mediated enhancement
663 of Legionella pneumophila-induced interleukin 1 activity. *Infect Immun* **61**, 4027-4032
664 (1993).
665 83. S. A. Miles, S. M. Conrad, R. G. Alves, S. M. Jeronimo, D. M. Mosser, A role for IgG
666 immune complexes during infection with the intracellular pathogen Leishmania. *J Exp*
667 *Med* **201**, 747-754 (2005).
668 84. P. E. Kima *et al.*, Internalization of Leishmania mexicana complex amastigotes via the
669 Fc receptor is required to sustain infection in murine cutaneous leishmaniasis. *J Exp*
670 *Med* **191**, 1063-1068 (2000).
671 85. P. Brodin *et al.*, Functional analysis of early secreted antigenic target-6, the dominant T-
672 cell antigen of Mycobacterium tuberculosis, reveals key residues involved in secretion,
673 complex formation, virulence, and immunogenicity. *J Biol Chem* **280**, 33953-33959
674 (2005).

675 86. S. A. Stanley, S. Raghavan, W. W. Hwang, J. S. Cox, Acute infection and macrophage
676 subversion by Mycobacterium tuberculosis require a specialized secretion system. *Proc*
677 *Natl Acad Sci U S A* **100**, 13001-13006 (2003).
678 87. T. A. Bates *et al.*, ESAT-6 undergoes self-association at phagosomal pH and an ESAT-6
679 specific nanobody restricts M. tuberculosis growth in macrophages. *bioRxiv*, (2024).
680 88. C. Mehaffy, J. M. Ryan, N. A. Kruh-Garcia, K. M. Dobos, Extracellular Vesicles in
681 Mycobacteria and Tuberculosis. *Front Cell Infect Microbiol* **12**, 912831 (2022).
682 89. C. Liu *et al.*, Quantification of circulating Mycobacterium tuberculosis antigen peptides
683 allows rapid diagnosis of active disease and treatment monitoring. *Proc Natl Acad Sci U*
684 *S A* **114**, 3969-3974 (2017).
685 90. B. M. Gunn *et al.*, A Fc engineering approach to define functional humoral correlates of
686 immunity against Ebola virus. *Immunity* **54**, 815-828 e815 (2021).
687 91. C. P. Taborda, J. Rivera, O. Zaragoza, A. Casadevall, More is not necessarily better:
688 prozone-like effects in passive immunization with IgG. *J Immunol* **170**, 3621-3630
689 (2003).
690 92. R. L. Jurado, J. Campbell, P. D. Martin, Prozone phenomenon in secondary syphilis.
691 Has its time arrived? *Arch Intern Med* **153**, 2496-2498 (1993).
692 93. K. Goodner, F. L. Horsfall, The Protective Action of Type I Antipneumococcus Serum in
693 Mice : Iv. The Prozone. *J Exp Med* **64**, 369-375 (1936).
694 94. C. E. Barry, 3rd *et al.*, The spectrum of latent tuberculosis: rethinking the biology and
695 intervention strategies. *Nat Rev Microbiol* **7**, 845-855 (2009).
696 95. M. Musvosvi *et al.*, T cell receptor repertoires associated with control and disease
697 progression following Mycobacterium tuberculosis infection. *Nat Med* **29**, 258-269
698 (2023).
699 96. P. L. Lin, J. L. Flynn, Understanding latent tuberculosis: a moving target. *J Immunol* **185**,
700 15-22 (2010).
701 97. E. B. Irvine *et al.*, Robust IgM responses following intravenous vaccination with Bacille
702 Calmette-Guerin associate with prevention of Mycobacterium tuberculosis infection in
703 macaques. *Nat Immunol* **22**, 1515-1523 (2021).
704 98. S. Balu *et al.*, A novel human IgA monoclonal antibody protects against tuberculosis. *J*
705 *Immunol* **186**, 3113-3119 (2011).
706 99. E. Ishida *et al.*, Mucosal and systemic antigen-specific antibody responses correlate with
707 protection against active tuberculosis in nonhuman primates. *EBioMedicine* **99**, 104897
708 (2024).
709 100. K. Dijkman *et al.*, Pulmonary MTBVAC vaccination induces immune signatures
710 previously correlated with prevention of tuberculosis infection. *Cell Rep Med* **2**, 100187
711 (2021).
712 101. B. I. Restrepo *et al.*, Cross-sectional assessment reveals high diabetes prevalence
713 among newly-diagnosed tuberculosis cases. *Bull World Health Organ* **89**, 352-359
714 (2011).
715 102. E. P. Scully, Sex, gender and infectious disease. *Nat Microbiol* **7**, 359-360 (2022).
716 103. T. Oni *et al.*, Trilateral overlap of tuberculosis, diabetes and HIV-1 in a high-burden
717 African setting: implications for TB control. *Eur Respir J* **50**, (2017).
718 104. E. van Woudenbergh *et al.*, HIV Is Associated with Modified Humoral Immune
719 Responses in the Setting of HIV/TB Coinfection. *mSphere* **5**, (2020).
720 105. B. I. Restrepo, Diabetes and Tuberculosis. *Microbiol Spectr* **4**, (2016).
721 106. K. Tanigaki *et al.*, Hyposialylated IgG activates endothelial IgG receptor FcgammaRIIB
722 to promote obesity-induced insulin resistance. *J Clin Invest* **128**, 309-322 (2018).
723 107. S. Fischinger *et al.*, A Mycobacterium tuberculosis Specific IgG3 Signature of Recurrent
724 Tuberculosis. *Front Immunol* **12**, 729186 (2021).

725 108. E. R. Haycroft *et al.*, Antibody glycosylation correlates with disease progression in SIV-
726 Mycobacterium tuberculosis coinfected cynomolgus macaques. *Clin Transl Immunology*
727 **12**, e1474 (2023).
728 109. K. Ronacher *et al.*, Acquired immunodeficiencies and tuberculosis: focus on HIV/AIDS
729 and diabetes mellitus. *Immunol Rev* **264**, 121-137 (2015).
730 110. J. G. Burel *et al.*, IgG glycosylation associates with risk of progression from latent to
731 active tuberculosis. *J Infect* **88**, 106115 (2024).
732 111. S. Ahangarzadeh, M. Bandehpour, B. Kazemi, Selection of single-chain variable
733 fragments specific for Mycobacterium tuberculosis ESAT-6 antigen using ribosome
734 display. *Iran J Basic Med Sci* **20**, 327-333 (2017).
735 112. E. P. Brown *et al.*, High-throughput, multiplexed IgG subclassing of antigen-specific
736 antibodies from clinical samples. *J Immunol Methods* **386**, 117-123 (2012).
737 113. E. H. Adhikari *et al.*, Diverging Maternal and Cord Antibody Functions From SARS-CoV-
738 2 Infection and Vaccination in Pregnancy. *J Infect Dis* **229**, 462-472 (2024).
739 114. A. E. Mahan *et al.*, A method for high-throughput, sensitive analysis of IgG Fc and Fab
740 glycosylation by capillary electrophoresis. *J Immunol Methods* **417**, 34-44 (2015).
741 115. C. Varadi, C. Lew, A. Guttman, Rapid magnetic bead based sample preparation for
742 automated and high throughput N-glycan analysis of therapeutic antibodies. *Anal Chem*
743 **86**, 5682-5687 (2014).
744 116. E. P. Brown *et al.*, Multiplexed Fc array for evaluation of antigen-specific antibody
745 effector profiles. *J Immunol Methods* **443**, 33-44 (2017).
746 117. T. Neuber *et al.*, Characterization and screening of IgG binding to the neonatal Fc
747 receptor. *MAbs* **6**, 928-942 (2014).
748 118. M. E. Ackerman *et al.*, A robust, high-throughput assay to determine the phagocytic
749 activity of clinical antibody samples. *J Immunol Methods* **366**, 8-19 (2011).
750 119. P. A. Darrah *et al.*, Multifunctional TH1 cells define a correlate of vaccine-mediated
751 protection against Leishmania major. *Nat Med* **13**, 843-850 (2007).
752 120. S. Jegaskanda *et al.*, Cross-reactive influenza-specific antibody-dependent cellular
753 cytotoxicity antibodies in the absence of neutralizing antibodies. *J Immunol* **190**, 1837-
754 1848 (2013).
755

756

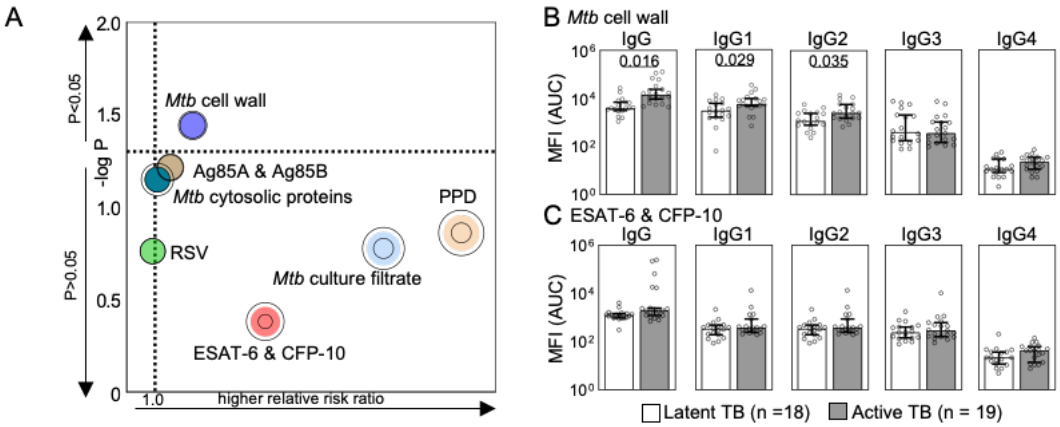

Figure 1. Antigen specificity changes how IgG associates with latent and active TB. (A) The bubble plot shows the capacity of each antigen specific IgG to predict active TB disease and latent TB infection by relative risk ratios (RRR) and 95% CI (rings), with higher likelihood of active TB >1 and latent TB <1. The median and 95% CI of IgG reactive to **(B)** *Mtb* cell wall and **(C)** ESAT-6 & CFP-10 are shown with *P*-values adjusted for sex and age.

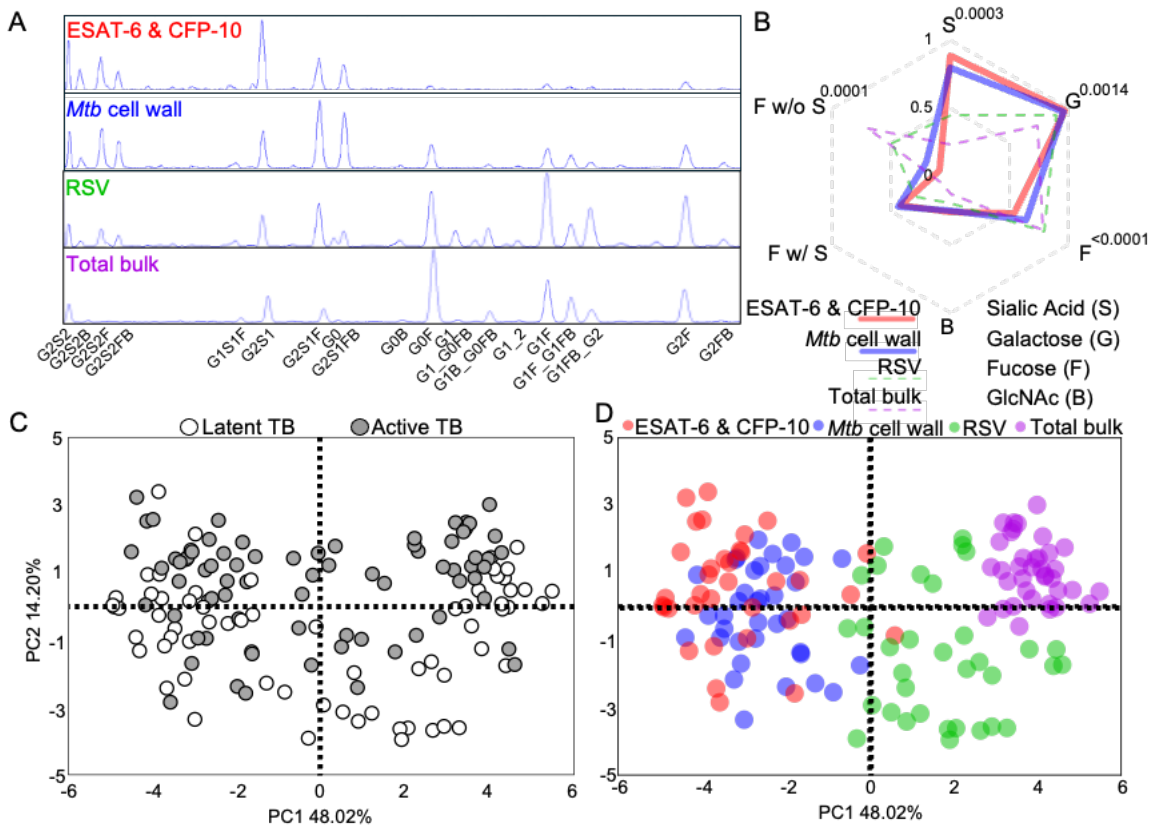

Figure 2. Antigen specificity separates antibody Fc domain glycosylation in latent and active TB. (A) Representative chromatograms show the patterns of individual glycoform isolated from the Fc domain of antigen specific and bulk total IgG in an individual TB patient sample. **(B)** The radar plot shows the relative abundance of total glycans from antigen specific and bulk total IgG with lines depicting the median of all TB patient samples. Comparisons between ESAT-6 & CFP-10 and *Mtb* cell wall IgG glycans were made by Wilcoxon matched-pairs signed-ranks tests and significance after adjustment for multiple comparisons is shown. **(C – D)** Principal components analysis was performed. Each dot summarizes the individual glycoforms for ESAT-6 & CFP-10, *Mtb* cell, RSV, or total bulk IgG for each individual TB patient. Score plots show clustering of glycosylation patterns with respect to **(C)** latent and active TB and **(D)** antigen specificity.

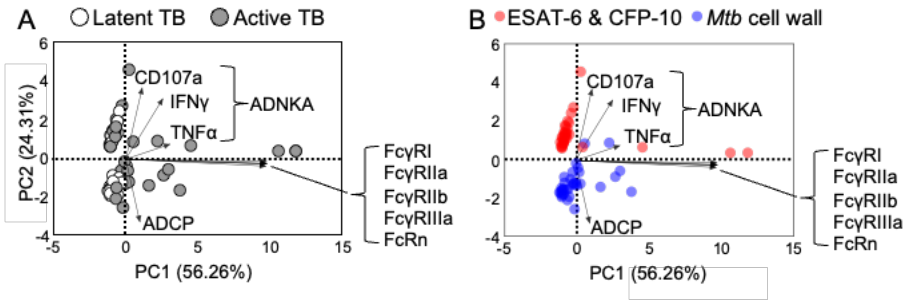

Figure 3. Antibody Fc effector functions diverge more by antigen specificity than latent and active TB. Principal components analysis was performed. Each dot summarizes the linear combination of the Fc receptor binding and Fc effector functions (antibody dependent natural killer cell activation (ADNKA) and antibody dependent cellular phagocytosis (ADCP)) for ESAT-6 & CFP-10 and *Mtb* cell wall IgG in each individual TB patient. Biplots show the distribution of individual TB patient profiles of Fc receptor binding and Fc effector functions to *Mtb* cell wall and ESAT-6 & CFP-10 with respect to **(A)** latent and active TB and **(B)** antigen specificity. The arrows in the loadings show the direction of the Fc features and functions that define the model.

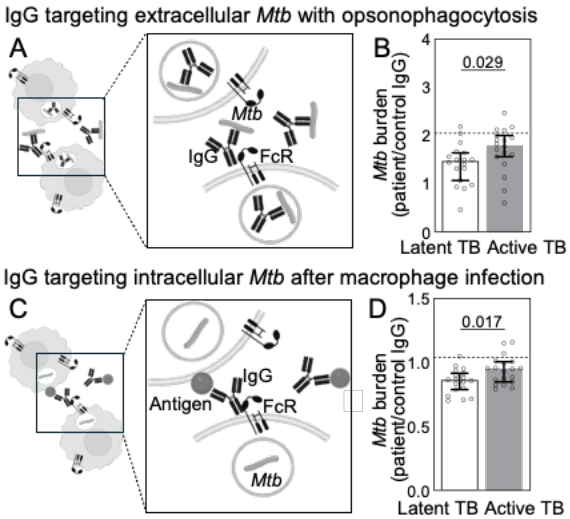

Figure 4. Latent and active TB IgG differentially impact extracellular and intracellular *Mtb* in macrophage infection. (A) To test the effect of antibodies on extracellular *Mtb*, IgG isolated from each TB patient was used to opsonize an *Mtb* H37Rv luminescent reporter strain to infect primary human monocyte derived macrophages (MOI=1). **(B)** Each dot represents *Mtb* burden relative to control IgG for each individual TB patient averaged over three different human macrophage donors in independent experiments. Median and 95% CI are shown. The dashed line shows the median of endemic control samples. **(C)** To test the effect of antibodies on intracellular *Mtb*, macrophages were first infected with the virulent *Mtb* H37Rv luminescent reporter strain, extracellular bacteria washed away, *Mtb* infected macrophages treated with IgG, and then **(D)** *Mtb* burden quantitated as in **(B)**. *P*-values are adjusted for sex and age.

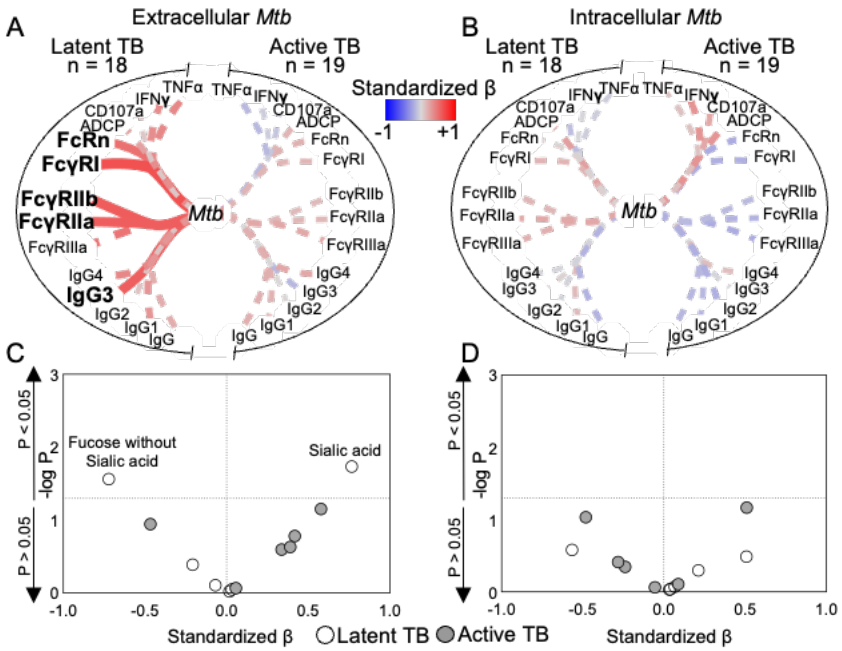

Figure 5. *Mtb* cell wall IgG enhances opsonophagocytosis of extracellular *Mtb*. The relationships between *Mtb* cell wall IgG features and *Mtb* were determined by simple linear regression in latent (n = 18) and active (n = 19) TB with respect to IgG mediated opsonophagocytosis of extracellular *Mtb* **(A)** and IgG targeting intracellular *Mtb* after macrophage infection **(B)**. Line thickness is inversely proportional to the *P*-value with <0.05 represented by solid lines. The effect of glycans from *Mtb* cell wall IgG on extracellular **(C)** and intracellular **(D)** *Mtb* was determined by multiple linear regression with IgG subclasses (Supplemental Tables 1 and 2). Volcano plots show the strength and direction of the link between *Mtb* cell wall IgG glycans and *Mtb* by standardized β.

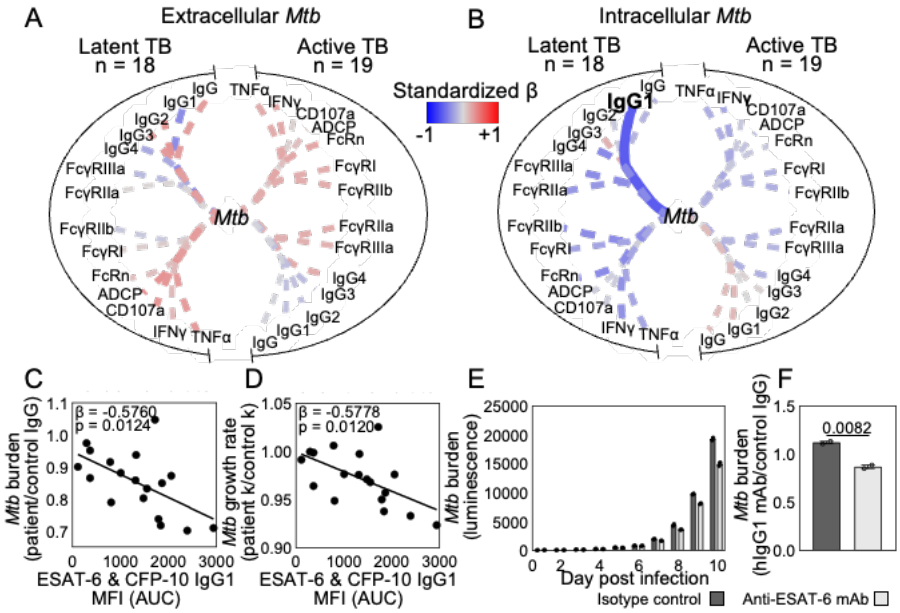

Figure 6. ESAT-6 & CFP-10 IgG inhibits intracellular *Mtb*. The relationships between ESAT-6 & CFP-10 IgG features and *Mtb* were determined by simple linear regression in latent (n = 18) and active (n = 19) TB with respect to IgG mediated opsonophagocytosis of extracellular *Mtb* **(A)** and IgG targeting intracellular *Mtb* after macrophage infection **(B)**. Line thickness is inversely proportional to the *P*-value with <0.05 represented by the solid line. Dot plots show the dependence of intracellular *Mtb* **(C)** burden and **(D)** growth rate on ESAT-6 & CFP-10 IgG1 in latent TB. **(E)** Intracellular *Mtb* burden after treatment with a monoclonal hIgG1 reactive to ESAT-6 & CFP-10 (anti-ESAT-6 mAb) and isotype control are shown for each day post infection by mean and SEM. **(F)** *Mtb* burden relative to control IgG is shown and unpaired t-test used to evaluate significance.

825 **Table: Cohort characteristics**

	Latent TB	Active TB	Significance	Endemic Controls
Total number of individuals	18	19		8
Age in years (range [median])	23 – 79 (40)	18 – 82 (38)	$P = 0.5730^{A}$	30 – 65 (47)
Sex (no. [%])			$P = 0.6185^{B}$	
Female	10 (56%)	9 (47%)		5 (63%)
Male	8 (44%)	10 (53%)		3 (38%)
BCG vaccination	15 (83%)	16 (84%)	$P = 0.9423^{C}$	7 (88%)

826
827 [A]Mann-Whitney U test was used to evaluate ages and [B,C]Chi-square test for sex and BCG
828 vaccination.
829
830

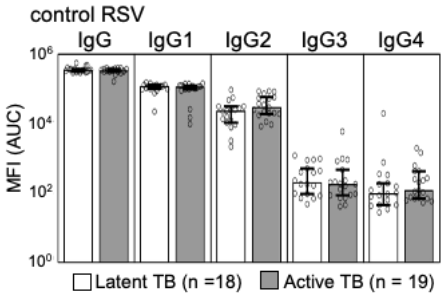

Supplemental Figure 1. No difference in RSV specific IgG between latent and active TB. Bar graphs show the median and 95% CI of IgG reactive to RSV. No *P*-values adjusted for sex and age were ≤ 0.05.

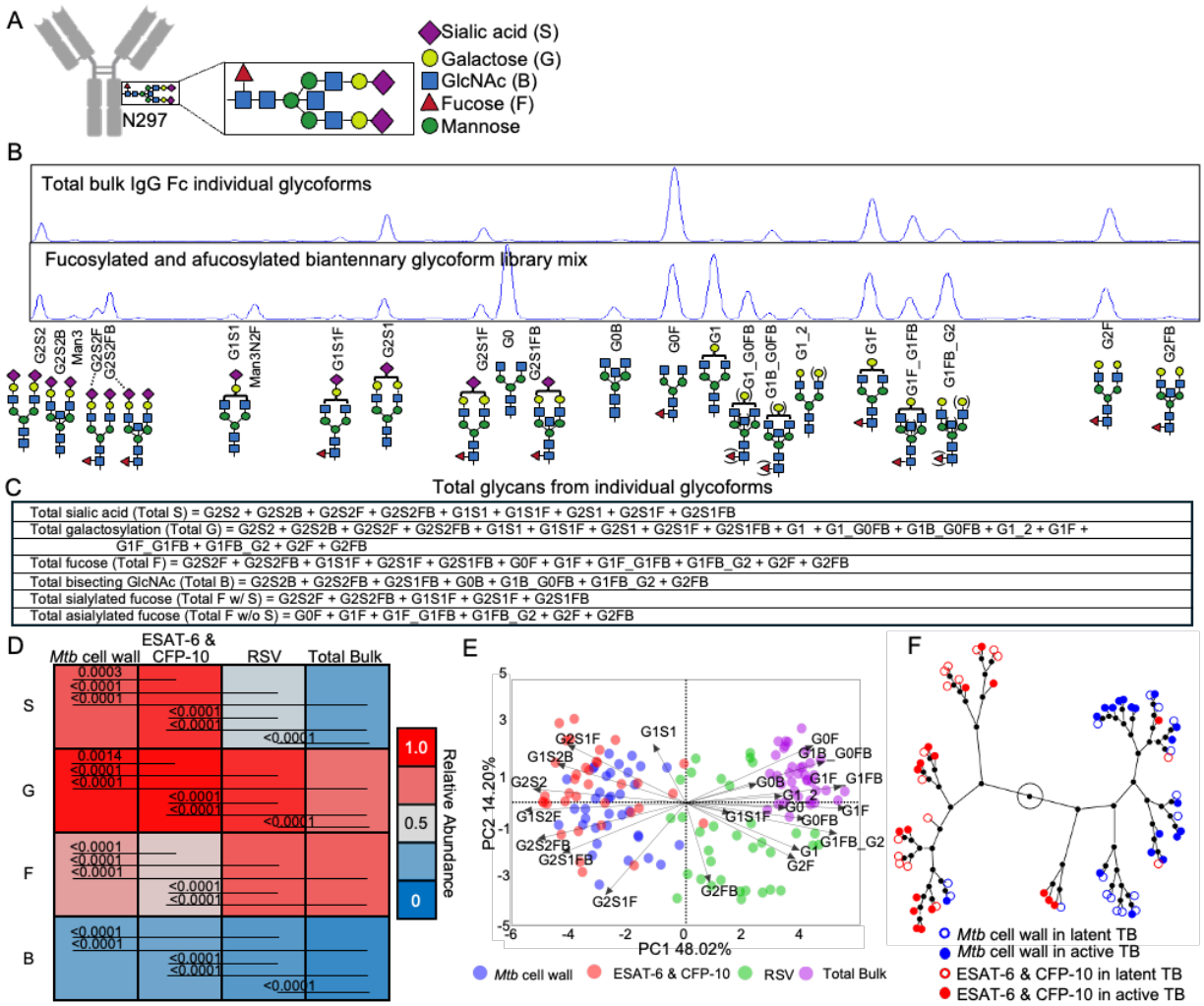

Supplemental Figure 2. Antigen specificity impacts IgG Fc domain N-glycosylation. (A) The conserved N297-linked complex biantennary glycan structure of the IgG Fc domain is shown. **(B)** Individual glycoforms on polyclonal IgG are quantified by capillary electrophoresis using standards from libraries. **(C)** Total glycans summarize individual glycoforms. **(D)** Heatmap shows the relative abundance of total glycans by antigen specificity. Comparisons were made by Wilcoxon matched-pairs signed rank tests and adjusted for multiple comparisons. **(E)** The biplot shows the distribution of individual TB patient glycoform patterns for *Mtb* cell wall, ESAT-6 & CFP-10, RSV, and total bulk IgG. The arrows in the loadings show the direction of the individual glycoforms that define the model. **(F)** The constellation plot shows the relationships between the glycan patterns for ESAT6 & CFP10 and *Mtb* cell wall IgG in each individual TB patient as determined by hierarchical clustering.

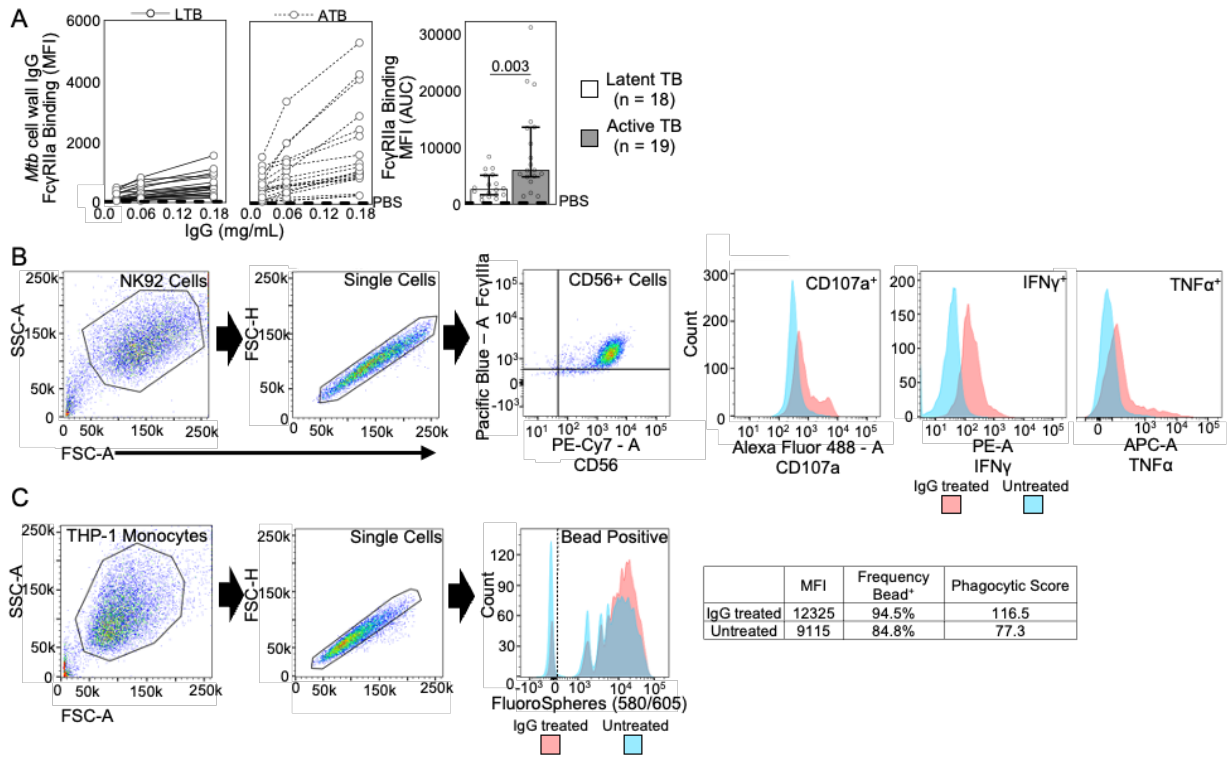

	MFI	Frequency Bead+	Phagocytic Score
IgG treated	12325	94.5%	116.5
Untreated	9115	84.8%	77.3

Supplemental Figure 3. Binding to Fc receptors, antibody dependent natural killer cell activation (ADNKA), and antibody dependent cellular phagocytosis (ADCP) was determined for each individual TB patient sample for *Mtb* cell wall and ESAT-6 & CFP-10. (A) Customized Luminex assays were used to measure antigen specific IgG-FcγR binding for each TB patient sample across three dilutions. *Mtb* cell wall IgG binding to FcγIIa plots are shown as examples. Area under the curve (AUC) of the MFI are determined for each individual TB patient and depicted in bar graphs with the median and 95% CI and significance adjusted for sex and age. **(B)** Antigen specific antibody dependent NK cell activation (ADNKA) was determined for each individual patient sample using the NK92 expressing FcγRIIIa cell line and antigen adsorbed ELISA plates. CD107a, IFNg, and TNFa on CD56+ cells were used to measure activation. **(C)** Antibody dependent cellular phagocytosis (ADCP) was quantified for each individual patient sample using THP-1 monocytes and antigen adsorbed fluorescent beads. The phagocytic score was calculated as the integrated MFI (%frequency x MFI/10,000).

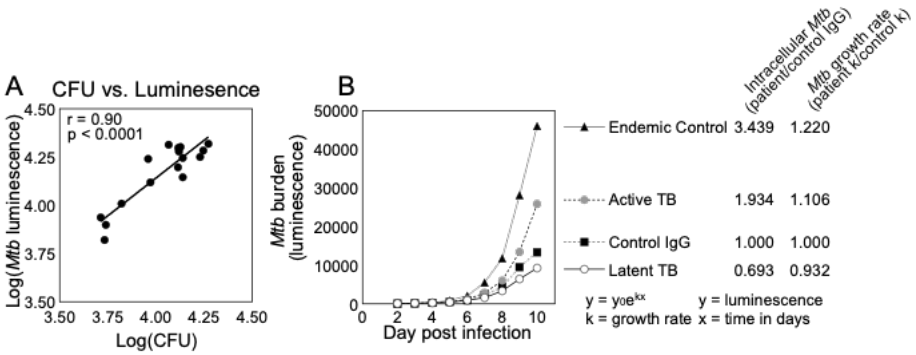

Supplemental Figure 4. The virulent *Mtb* H37Rv luminescent reporter strain captures differences in bacterial growth and burden between treatment with latent and active TB IgG. (A) Pearson correlation was used to link luminescence and CFU. **(B)** Daily luminescence measurements of *Mtb* infected macrophages enable the determination of bacterial burden and growth rate by the exponential growth model.

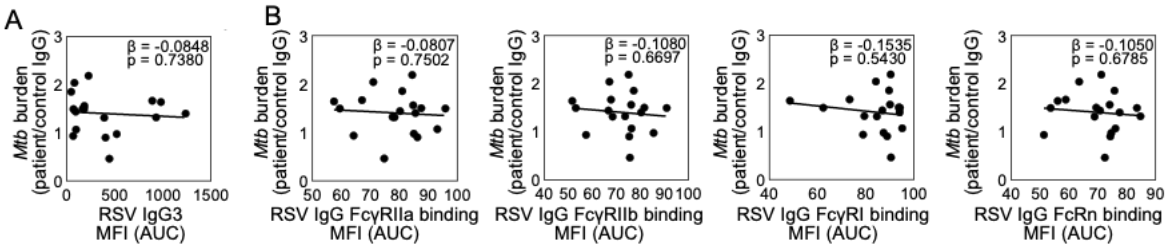

Supplemental Figure 5. RSV IgG3 and Fc receptor binding do not relate to extracellular *Mtb*. The absence of significant relationships between *Mtb* burden after IgG mediated opsonophagocytosis of extracellular bacteria and **(A)** RSV IgG3 and **(B)** RSV IgG Fc receptor binding was determined by linear regression.

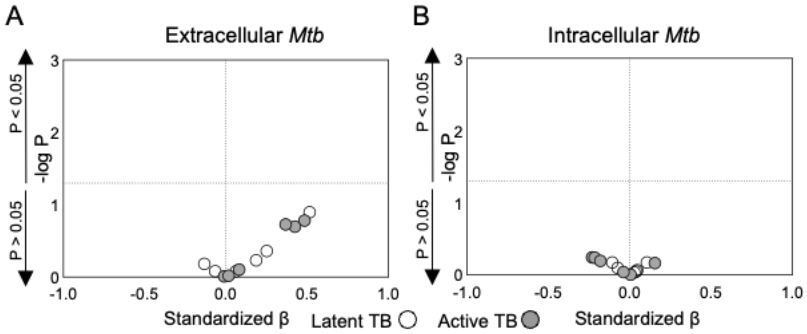

Supplemental Figure 6. ESAT-6 & CFP-10 glycans do not relate to *Mtb* burden. The effect of glycans from ESAT-6 & CFP-10 IgG on extracellular (A) and intracellular (B) Mtb was determined by multiple linear regression with IgG subclasses (Supplemental Tables 3 and 4). Volcano plots show the strength and direction of the link between ESAT-6 & CFP-10 IgG glycans and *Mtb* by standardized β.

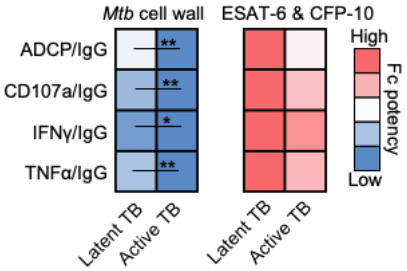

Supplemental Figure 7. *Mtb* cell wall, not ESAT-6 & CFP-10, IgG Fc potency is higher in latent compared to active TB. The heatmap shows the amount of antigen specific Fc effector functions relative to IgG titers with significance adjusted for sex and age. *$P \leq 0.05$ and **$P \leq 0.01$.

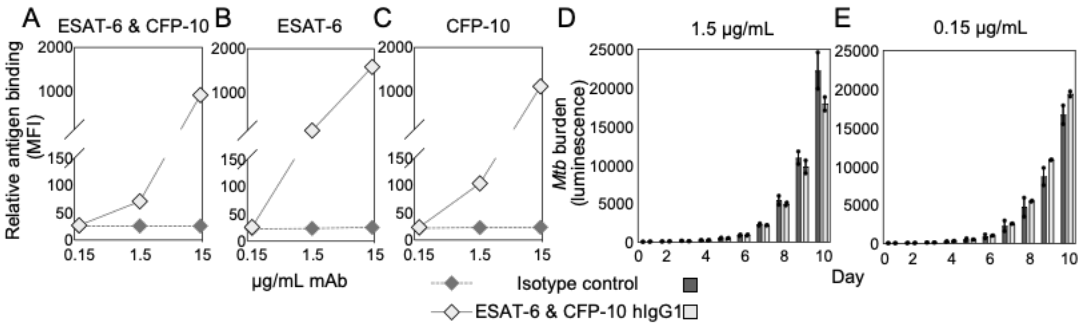

Supplemental Figure 8. A human IgG1 mAb binds ESAT-6 & CFP-10 and does not inhibit intracellular *Mtb* at low doses. Relative binding of mAb to ESAT-6 and isotype control CR3022 (anti-SARS-CoV-2 RBD hIgG1) to **(A)** ESAT-6 & CFP-10, **(B)** ESAT-6, and **(C)** CFP-10 are shown. Treatment of *Mtb* infected macrophages with **(D)** 1.5 or **(E)** 0.15µg/mL mAb did not significantly impact *Mtb* burden compared to isotype control as determined by unpaired t-test. Mean and SEM are shown.

901 **Supplemental Table 1. Models evaluating the impact of *Mtb* cell wall IgG glycans and**
902 **subclasses on extracellular *Mtb***
903
904 Latent TB

Model Glycan	Glycan Std. β / *P*-value	IgG1 Std. β / *P*-value	IgG2 Std. β / *P*-value	IgG3 Std. β / *P*-value	IgG4 Std. β / *P*-value	Model *P*-value
Sialic Acid	0.77 / 0.0184	0.64 / 0.0247	-0.32 / 0.1595	0.52 / 0.0082	0.81 / 0.0071	0.0085
Galactose	0.02 / 0.9423	0.16 / 0.5015	-0.21 / 0.4593	0.54 / 0.0276	0.47 / 0.1421	0.1074
Fucose	-0.21 / 0.4081	0.24 / 0.3317	-0.28 / 0.3255	0.53 / 0.0269	0.54 / 0.0804	0.0801
GlcNAc	-0.07 / 0.7791	0.15 / 0.5321	-0.23 / 0.4314	0.52 / 0.0387	0.49 / 0.1177	0.1041
Fucose w/ S	0.03 / 0.8859	0.15 / 0.5039	-0.20 / 0.4992	0.54 / 0.0265	0.46 / 0.1209	0.1067
Fucose w/o S	-0.72 / 0.0273	0.60 / 0.0350	-0.31 / 0.1786	0.54 / 0.0084	0.79 / 0.0097	0.0118

905
906 Active TB

Sialic Acid	0.42 / 0.1653	0.27 / 0.3103	0.17 / 0.6448	-0.07 / 0.8632	0.34 / 0.2314	0.5379
Galactose	0.58 / 0.0703	0.30 / 0.2434	0.08 / 0.8159	0.13 / 0.7475	0.41 / 0.1466	0.3426
Fucose	0.06 / 0.8568	0.20 / 0.5014	0.25 / 0.5244	-0.25 / 0.5229	0.20 / 0.4926	0.8653
GlcNAc	0.34 / 0.2528	0.16 / 0.5719	0.28 / 0.4431	-0.18 / 0.6257	0.18 / 0.4939	0.6441
Fucose w/ S	0.39 / 0.2324	0.15 / 0.5732	0.27 / 0.4592	-0.08 / 0.8360	0.27 / 0.3356	0.6232
Fucose w/o S	-0.47 / 0.1127	0.31 / 0.2503	0.21 / 0.5463	-0.09 / 0.8134	0.34 / 0.2165	0.4453

907
908
909 Std. β – Standardized Beta from multiple linear regression
910

911 **Supplemental Table 2. Models evaluating the impact of *Mtb* cell wall IgG glycans and**
912 **subclasses on intracellular *Mtb***
913
914 Latent TB

Model Glycan	Glycan Std. β / *P*-value	IgG1 Std. β / *P*-value	IgG2 Std. β / *P*-value	IgG3 Std. β / *P*-value	IgG4 Std. β / *P*-value	Model *P*-value
Sialic Acid	0.51 / 0.3237	0.48 / 0.2933	-0.17 / 0.6513	0.01 / 0.9808	0.22 / 0.6167	0.9124
Galactose	0.03 / 0.9234	0.16 / 0.6200	-0.10 / 0.7947	0.02 / 0.9590	0.01 / 0.9786	0.9962
Fucose	0.04 / 0.9149	0.14 / 0.6933	-0.08 / 0.8396	0.02 / 0.9437	-0.02 / 0.9642	0.9961
GlcNAc	0.07 / 0.8453	0.17 / 0.6096	-0.08 / 0.8539	0.04 / 0.9050	-0.03 / 0.9411	0.9953
Fucose w/ S	0.21 / 0.5005	0.16 / 0.6218	-0.03 / 0.9440	0.04 / 0.9009	-0.02 / 0.9646	0.9708
Fucose w/o S	-0.57 / 0.2627	0.51 / 0.2528	-0.18 / 0.6286	0.02 / 0.9544	0.25 / 0.5675	0.8713

915
916 Active TB

Sialic Acid	-0.48 / 0.2668	-0.28 / 0.3274	-0.28 / 0.8464	-0.06 / 0.9620	-0.01 / 0.0928	0.4236
Galactose	-0.24 / 0.3572	-0.26 / 0.3098	-0.31 / 0.9483	0.02 / 0.8013	0.07 / 0.4499	0.7991
Fucose	0.09 / 0.4065	-0.24 / 0.3544	-0.30 / 0.6194	0.16 / 0.5731	0.16 / 0.7775	0.8782
GlcNAc	-0.05 / 0.4609	-0.21 / 0.3204	-0.33 / 0.6755	0.13 / 0.5665	0.16 / 0.8595	0.8854
Fucose w/ S	-0.28 / 0.5320	-0.17 / 0.2391	-0.37 / 0.9574	0.02 / 0.6960	0.11 / 0.3861	0.7680
Fucose w/o S	0.51 / 0.2129	-0.32 / 0.2324	-0.33 / 0.9108	-0.03 / 0.9928	0.00 / 0.0681	0.3564

917
918 Std. β – Standardized Beta from multiple linear regression
919
920

921 **Supplemental Table 3. Models evaluating the impact of ESAT-6 & CFP-10 IgG glycans**
922 **and subclasses on extracellular *Mtb***
923
924 Latent TB

Model Glycan	Glycan Std. β / *P*-value	IgG1 Std. β / *P*-value	IgG2 Std. β / *P*-value	IgG3 Std. β / *P*-value	IgG4 Std. β / *P*-value	Model *P*-value
Sialic Acid	-0.06 / 0.8243	-0.28 / 0.4560	0.12 / 0.6978	0.21 / 0.5683	-0.11 / 0.7394	0.6554
Galactose	-0.13 / 0.6518	-0.27 / 0.4679	0.12 / 0.6804	0.23 / 0.5203	-0.09 / 0.7722	0.6277
Fucose	0.25 / 0.4371	-0.18 / 0.6237	0.19 / 0.5342	0.26 / 0.4699	-0.22 / 0.5219	0.5578
GlcNAc	0.52 / 0.1263	-0.12 / 0.7356	0.32 / 0.2837	0.27 / 0.3953	-0.33 / 0.3054	0.3088
Fucose w/ S	0.19 / 0.5876	-0.19 / 0.6347	0.17 / 0.5789	0.20 / 0.5730	-0.20 / 0.5746	0.6116
Fucose w/o S	0.06 / 0.8270	-0.28 / 0.4555	0.11 / 0.7011	0.20 / 0.5690	-0.11 / 0.7347	0.6556

925
926 Active TB

Sialic Acid	-0.01 / 0.9785	0.22 / 0.5553	-2.41 / 0.1041	1.95 / 0.1656	0.56 / 0.1603	0.4468
Galactose	0.08 / 0.7855	0.24 / 0.4999	-2.23 / 0.1436	1.79 / 0.2180	0.54 / 0.1707	0.4014
Fucose	0.49 / 0.1644	-0.14 / 0.7289	-2.85 / 0.0379	2.51 / 0.0636	0.42 / 0.2529	0.2195
GlcNAc	0.43 / 0.1998	-0.13 / 0.7563	-2.05 / 0.1185	2.01 / 0.1137	0.40 / 0.2949	0.2458
Fucose w/ S	0.37 / 0.1875	0.00 / 0.9981	-2.30 / 0.0779	2.10 / 0.1004	0.45 / 0.2165	0.2371
Fucose w/o S	0.02 / 0.9596	0.21 / 0.5565	-2.42 / 0.1004	1.95 / 0.1618	0.55 / 0.1611	0.4465

927
928 Std. β – Standardized Beta from multiple linear regression
929

930 **Supplemental Table 4. Models evaluating the impact of ESAT-6 & CFP-10 IgG glycans**
931 **and subclasses on intracellular *Mtb***
932
933 Latent TB

Model Glycan	Glycan Std. β / *P*-value	IgG1 Std. β / *P*-value	IgG2 Std. β / *P*-value	IgG3 Std. β / *P*-value	IgG4 Std. β / *P*-value	Model *P*-value
Sialic Acid	0.11 / 0.6710	-0.51 / 0.1236	-0.26 / 0.3071	-0.08 / 0.8015	-0.26 / 0.3521	0.1933
Galactose	0.05 / 0.8519	-0.53 / 0.1126	-0.27 / 0.3022	-0.06 / 0.8370	-0.25 / 0.3668	0.2049
Fucose	-0.07 / 0.7971	-0.55 / 0.1119	-0.29 / 0.2917	-0.07 / 0.8271	-0.22 / 0.4692	0.2024
GlcNAc	0.03 / 0.9208	-0.52 / 0.1323	-0.25 / 0.3753	-0.04 / 0.8884	-0.26 / 0.3989	0.2070
Fucose w/ S	0.04 / 0.8910	-0.51 / 0.1523	-0.25 / 0.3533	-0.05 / 0.8780	-0.26 / 0.3918	0.2062
Fucose w/o S	-0.11 / 0.6694	-0.51 / 0.1252	-0.26 / 0.3111	-0.08 / 0.8020	-0.26 / 0.3558	0.1932

934
935 Active TB

Sialic Acid	0.16 / 0.6853	-0.21 / 0.6004	0.73 / 0.6406	-0.48 / 0.7478	-0.12 / 0.7744	0.9601
Galactose	0.01 / 0.9879	-0.26 / 0.5207	0.53 / 0.7462	-0.34 / 0.8304	-0.13 / 0.7662	0.9745
Fucose	-0.23 / 0.5701	-0.09 / 0.8499	0.73 / 0.6292	-0.60 / 0.6939	-0.06 / 0.8827	0.9435
GlcNAc	-0.22 / 0.5759	-0.09 / 0.8613	0.34 / 0.8182	-0.37 / 0.7994	-0.05 / 0.9159	0.9446
Fucose w/ S	-0.04 / 0.9107	-0.24 / 0.5816	0.51 / 0.7306	-0.35 / 0.8132	-0.12 / 0.7886	0.9735
Fucose w/o S	-0.18 / 0.6371	-0.21 / 0.6033	0.74 / 0.6299	-0.49 / 0.7423	-0.12 / 0.7816	0.9543

936
937 Std. β – Standardized Beta from multiple linear regression
938
939
940
941

942